Master Thesis

Investigation of the Refractive Index of Combustion Engines Fuels for Applications in Spray Diagnostics

by

Vitor Hugo Fernandes

Department of Applied Mechanics
Division of Combustion
Chalmers University of Technology
Göteborg , Sweden, 2008

Abstract

In now-a-days the research in new automotive Engine systems as Direct Injection Gasoline is a priority task .Direct Injection Gasoline Engines have revealed as a promising technology to reduce fuel consumption and gas emissions, however its success is dependent on achieving a good fuel distribution in the cylinder. For this purpose, advanced spray diagnostic methods are required, and Phase-Doppler anemometry is one important method that can provide data on drop size and velocity in a spray. For accurate measurements the knowledge of the refractive index and also its dependence on surroundings environmental conditions, as the temperature and pressure, is still required.

The purpose of this work is to study the dependence of the refractive index on the major factors influencing its behavior in the typical conditions of an engine, and that means temperature, pressure and composition. To study this parameters a new setup was designed and several experimental works were carried out. The refractive index is determined by measuring the deflection of a beam from an Argon-Ion laser that passes through a refraction cell containing the fuel to be studied. The refraction cell is constituted by a 45^{o} holly prism and a temperature controller that allows reaching higher temperatures, this refraction cell can also be placed inside a pressure chamber where higher pressures can be reached.

The experimental work was divided into three parts. In the first part the refractive index of several fuels including Isooctane, Gasoline, Diesel, E85, E95, and others of typical usage in internal combustion engines was measure at ambient conditions. In the second part of the study we have done a study of the pressure and temperature influence on the refractive index. The third and last experimental work was study the composition effect in the refractive index. With the increasing pressure we measured an apparent decrease of the refractive index due to the larger increase of the refractive index of air when compared to the fuel. For temperature we verified a linear decrease of the refractive index. When heating and cooling multi-components we notice an irreversible increase in the refractive index that we later confirmed that was caused by the composition change.

List of Symbols

$\mathbf{v_i}$ - velocity of the wave in the incident medium

$\mathbf{v_t}$ – velocity of the wave in the transmitted medium

$\mathbf{n_i}$ - Refractive Index of the incident medium

$\boldsymbol{n_t}$ – Refractive Index of the transmitted medium

$\boldsymbol{f}$ – Frequency of the wave.

$\boldsymbol{f_D}$ – Doppler frequency

$\boldsymbol{\lambda}$ - Wavelength

$\boldsymbol{\theta_{air\ in}}$ – Air incoming angle into the cuvette

$\boldsymbol{\theta_{air\ out}}$ - Air outgoing angle from the cuvette

$\boldsymbol{\theta_{fuel\ in}}$- Incoming angle inside the fuel

$\boldsymbol{\theta_{fuel\ out}}$ - Outgoing angle inside the fuel

$\boldsymbol{P}$ – Pressure

T - Temperature

$\boldsymbol{n}$ – Refractive Index

$\boldsymbol{n_{Rel.}}$ – Relative refractive Index between the surrounding medium and the droplet

$\boldsymbol{\Phi_{Refraction}}$ – Phase-shift from the refraction light

$\boldsymbol{\Phi_{Reflection}}$ - Phase-shift from the reflected light

$\boldsymbol{n'}$- Refractive Index calculated according to the relative measuring method

$\boldsymbol{n'_{10bar}}$ – average value of the *n'* for a pressure of 10 bar

$\boldsymbol{n'_{30bar}}$ - average value of the *n'* for a pressure of 30 bar

$\boldsymbol{S}$ – Standard deviation extended to 95% confidence

$\boldsymbol{U_i}$ – Total uncertainty of the variable i

$\boldsymbol{K}$ – Constant of expansion of the uncertainty confidence level

$\boldsymbol{B_i}$ – Random error of the variable i

$\boldsymbol{P_i}$ - Systematic error of the variable i

$\boldsymbol{a}$ – scale resolution of the utilized ruler

$\boldsymbol{x_i}$ – measured distance of the variable i

Contents

1. Introduction

The research in new technologic solutions for automotive engines has been part of the car-makers history; With the recent strong concerns about the environment (according to OECD the economic-environmental projections show that world green house gas emissions are expected to grow by 37% to 2030) and the increase of petrol price this become a priority issue. Due to these concerns both Diesel and Gasoline engines have suffered many improvements in the last years, in particular Gasoline Direct Injection Engines that since the advance of electronic control system in the nineties become a usable system with a big potential to reduce fuel consumption and gas emissions. However its potential it requires a great effort in research in order to tackle many problems, in particular a good fuel distribution, that are still affecting the success of this technology.

In engines research many optical techniques as Mie Scattering, Laser-induced Fluorescence, Rayleigh Scattering, Phase Doppler Anemometry, etc., are used to study fuel sprays; Among these techniques Phase Doppler Anemometry (PDA), used to evaluate the droplet size and fuel distribution, is one of the most important. Although there are other techniques as Malvern Particle Sizer or Laser Sheet Dropsizing, that can alsdo be used to measure the particle size, PDA had revealed the most well succeeded technique, but its usage requires some preconditions and one of them is the knowledge of the combined refractive index between the medium and the particle. However its importance, its usage in actual research applications is restricted to the knowledge of the droplets refractive index for some compositions and for ambient conditions.

As high temperatures and high pressures are parameters presented in the typical environmental conditions of droplets sizing, they might be important parameters affecting the refractive index of the combined medium air/fuel, which we should be concerned about.

Another limitation is the lack of knowledge about the refractive index for fuels that have conditioned their usage in Spray Injection research using the PDA system, leading to an obvious loss for Engines research.

In this work we are expecting to achieve an understanding about the refractive index and its major influence parameters, namely temperature, pressure and also composition, and also enlarge the knowledge about the refractive index of different types of fuels, namely Gasoline, E85, E95, Isooctane, Ethanol, Diesel, among others. In order to achieve this goal we also design and build the setup needed.

2. Background

2.1. Refractive Index

Per definition the refractive index or the index of refraction of a medium is the ratio between the phase velocity of wave propagation in a reference medium and the phase velocity in the medium itself [1]. It is mostly related with light and connected to the vacuum as reference medium (that for simplification normally is approximated by air). It is normally

denoted by *n* and its mathematical definition can be denoted by Eq.(2.1.), where *c* represents the speed of light in the vacuum.

$$n = \frac{c}{v_{medium}} \qquad \text{(Eq.2.1)}$$

For transparent and non magnetic materials the refractive index can also be determined by the interaction of a electrical field of the wave and the permittivity ε of the medium (Eq.2.2).The ε_0 is the permittivity of vacuum and it is equal to $10^7/(4\pi c_0^2)Fm^{-1}$ [1].

$$n = \sqrt{\varepsilon_r} = \sqrt{\frac{\varepsilon}{\varepsilon_0}} \qquad \text{(Eq.2.2)}$$

The refractive index is a number bigger than one, and normally lower than 1.7 (for normal fuels) in its more conventional notation is presented with a subscript that refers the wavelength used , (the most typical is sodium D (λ=589 nm) that is denoted by the latter D), and by a superscript that indicates the temperature.

2.1.1 Light and surface interference

When light (a wave) traveling through a certain medium intersects a surface (other medium), some of the light is reflected, some is transmitted and some may be absorbed (see Fig.2.1) ; For a specular surface the angle of reflection θ_r will be the same as the angle of incidence θ_i and this is known by the law of reflection.

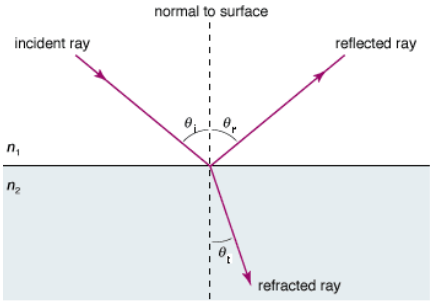

Figure 2.1- Reflection and Transmission at a Surface

The frequency of the light can be seen as the number of the wavefronts arriving at the interface per second, this implicates that the wavelength and the frequency of the reflected light is the same as the incident medium, but not the same wavelength as the transmitted, since for different mediums a wave has different propagation speeds, according to the resistance of the medium [2].

2.1.2 The Snell's Law

The transmitted light, also known as refracted light, not only has a different propagation speed v_t as it also has a different propagation angle θ_t this two things are related together and this relation is expressed by Eq.2.3.

$$\frac{\sin\theta_i}{v_i} = \frac{\sin\theta_t}{v_t} \qquad \text{(Eq.2.3)}$$

If we rearrange Eq. 2.3 and replace the propagation speed from the respective refractive index we will end with Eq.2.4 that is known by **Snell's law** or simply by Law of refraction [2].

$$n_i \sin\theta_i = n_t \sin\theta_t \qquad \text{(Eq.2.4)}$$

This equation is very useful because it correlates directly the refractive index with the propagation angle, not being needed to measure the propagation speed to determinate the refractive index of the medium.

In Snell's Law there are two extreme/exception cases, the first one is concerning an incoming angle of 0^o, in this case the transmitted light propagates without deflection; The second is concerning the total reflection, and that means that all light is reflected, this phenomenon happens when the ratio of n_t/n_i multiplied by the sin of incoming angle is bigger than one.

2.1.3 Light Dispersion

The refractive index for one same medium is a function of the wavelength, except for vacuum and this can be easily demonstrated. In free space (vacuum) the phase velocity *c*, is given by $c = f.\lambda_0$, where *f* is the wave frequency and λ_0 is the free-space wavelength, for other medium the velocity changes for $v = f.\lambda$, as the frequency does not change with medium this relation of the refractive index can also been written as $n = \lambda_0/\lambda$ [2]; So the refractive index normally decreases with the wavelength used (see Fig.2.2), and this is what causes a prism to divide with light in its different spectral colors (wavelengths), or the formation of rainbows, and is known as dispersion.

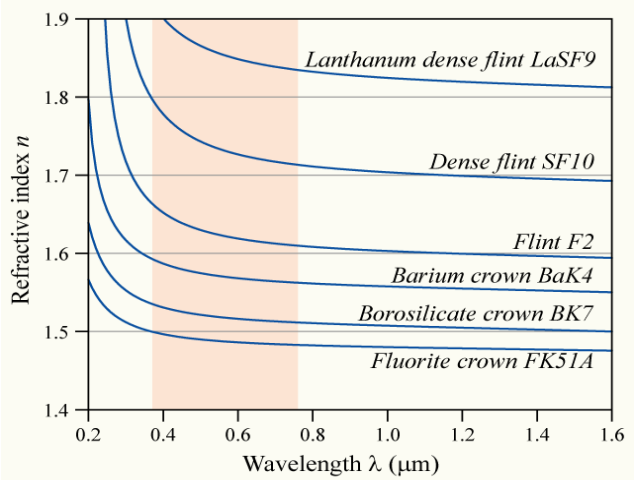

Figure2.1- Variation of the refractive index with the wavelength for different types of glasses

2.1.4 The Lorentz-Lorenz correlation

The Lorentz- Lorenz correlation, presented in Eq. 2.5 relates the refractive index of a pure liquid with its molecular proprieties: the electronic polarizability α, the molecular weight M, the density ρ, and the Avogadro's number N [3].

$$\frac{n^2-1}{n^2+2}=\frac{4\pi N}{3M}\rho\alpha \qquad \text{(Eq.2.5)}$$

The polarizability is…" the relative tendency of a charge distribution, like the electron cloud of an atom or molecule, to be distorted from its normal shape by an external electric field, which may be caused by the presence of a nearby ion or dipole". And is defined as the ratio of the induced dipole moment P of an atom to the electric field E that produces this dipole [4].

The Eq.2.5 takes into account the electrostatic interactions between molecular dipoles, but doesn't take into account the local interactions between a molecule and its neighbors due to the pressure and temperature, that has a non negligible influence on the electronic polarizability [3]. Consider these influences we can rewrite the Lorentz-Lorenz Correlation (Eq.2.6).

$$\frac{n^2-1}{n^2+2}=A\rho^B e^{-CT} \qquad \text{(Eq.2.6)}$$

In Eq.1.6 A, B and C are constants of the liquid. Constants B and C are expressed by Eq.2.7 and Eq.2.8.

$$B = 1 + \left(\frac{\partial \ln \alpha}{\partial \ln P} \right)_T \qquad \text{(Eq.2.7)} \qquad C = -\left(\frac{\partial \ln \alpha}{\partial T} \right)_P \qquad \text{(Eq.2.8)}$$

The Eq. 1.6 shows the dependence of the refractive index on the temperature and pressure, which is directly transduced by its influence on the electronic polarizability and indirectly to its influence on the density of the liquid.

Although the relevant importance on understanding the dependence of the refractive index on Temperature and pressure once its complexity is beyond the expectations of this thesis.

In the other side the Lorentz –Lorenz Correlation for gases and particularly for air (Eq.2.9) can be more useful to correlate the dependence of the refractive index of air with temperature and pressure [5].

$$\frac{n^2 - 1}{n^2 + 2} = \sum_{i=1}^{n} R_i \rho_i \qquad \text{(Eq.2.9)}$$

In Eq.2.9 ρ_i is the partial density and R_i is the specific refraction of the i component, that can be obtained by Eq.2.10, in which *N* is Avogadro's number, M_i the Molecular weight and α_i the polarizability of i component.

$$R_i = \frac{4}{3}\pi \left(\frac{N}{M_i} \right) \alpha_i \qquad \text{(Eq.2.10)}$$

2.1.5 Others Proprieties

- **Anisotropy:** for some substances the refractive index of a medium might differ with the direction of the light propagation and its polarization.
- **Nonlinearity:** the refractive index can change as light passes through it if a high intensity light, such as a laser beam, is used creating a nonlinear optics. If the variation is linear with the intensity it is called the Optical Kerr effect and origins phenomenon such as self-focusing.
- **Inhomogeneity:** a refractive index change with the position lead to a gradient-index medium, which can cause a bent or a focus of the light. This is an important propriety that is exploited to produce lenses.

2.1.6. Refractometer

Figure2.2- Abbe' Refractometer

A refractometer is an equipment used to measure the refractive index. The most common (commercial) equipment for laboratorial applications is the Abbé refractometer (see Fig.2.3), it measures the refractive index with a normal precision of 10^{-5}, however its usage is almost limited to ambient conditions.

2.2. Phase Doppler Anemometry

Phase Doppler Anemometry, PDA is a technique based on light scattering interferometer, and can be consider as an extension of Laser Doppler Anemometry LDA, once besides velocity it also allow to measure the particle size.

Phase Doppler Anemometry systems normally uses Argon-ion laser as light sources, and it normally operates in multi mode generating various light frequencies that can be decomposed.

The light coming from the laser source is divided in two beams that are frequency shift by a Bragg Cell and are next guided to the transmitter/emitter, that focus the two beams in a point on the space.

The intersection point of the two beams form a probe volume with alternated lists pattern (also known by fringes) of high and low intensity light (see fig.2.4).

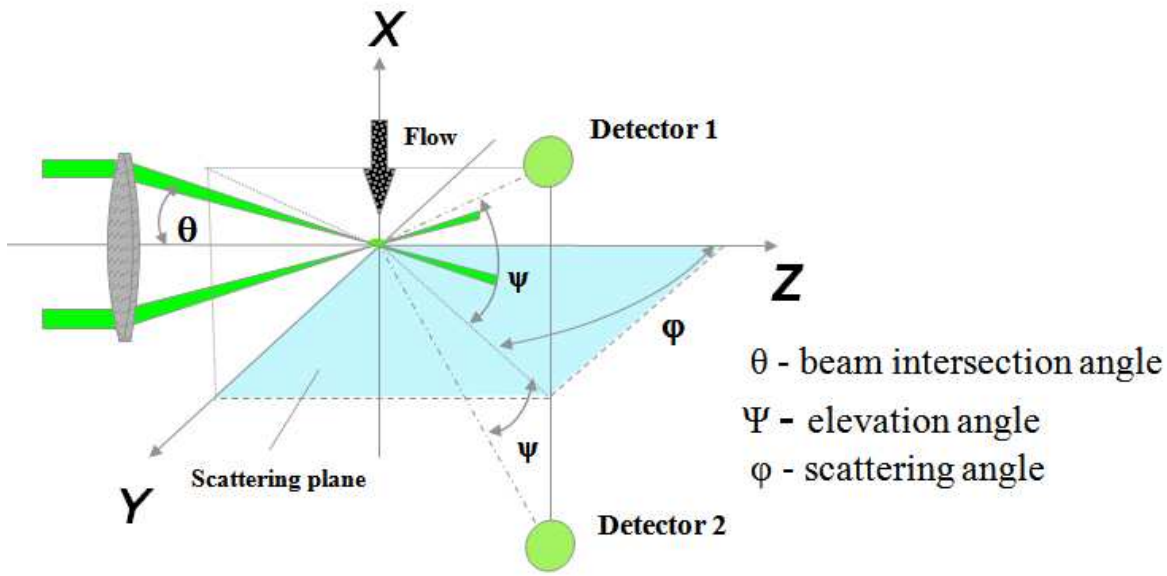

Figure2.3 -PDA geometrical description

The light scattered by the particles crossing the probe volume is captured by a receiver displaced in a plane rotated φ (scattering angle) from the plane containing the two beams, and then converted to an electrical signal by photomultiplier tubes (PMTs).

2.2.1. Velocity measuring

A particle moving in a direction perpendicular to the plane of the two beams crosses through the probe volume and scattered the light, this provokes a fluctuation of the light intensity with a frequency proportional to the particle velocity (Eq.2.11). The constant of proportionality is the distance between consecutive light fringes d_D which can be calculated from the beam's frequency f_D and the beam's focus angle θ [6].

$$u = f_D \cdot d_D \qquad \text{(Eq.2.11)}$$

The frequency shift of the two beams originates a movement of the interference fringes, allowing to distinguished positive from negative velocities (see fig.2.5)

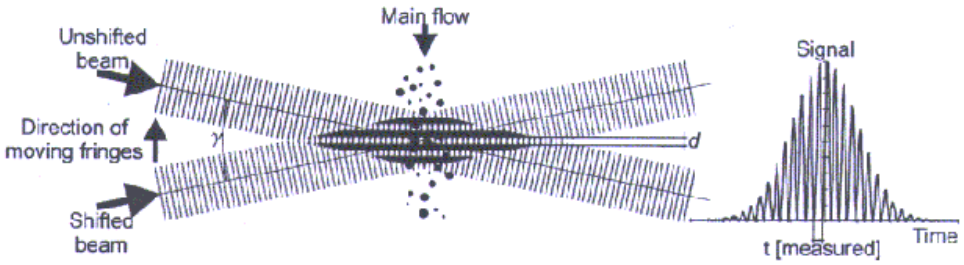

Figure 2.4 - probe volumm and particle velocity measuring. The diagram shows the received signal.

If another component of the velocity needs to be measure another pair of beams (of a different wavelength) in a perpendicular plan to that component velocity, should be used.

2.2.2. Diameter measuring

In order to explain the diameter measuring process we should first of all explain the light-scattering phenomenon.

When the light run into the outside surface of a partially transparent droplet some part is reflected, and another is transmitted. The transmitted light is deflected from an angle that is related to the refractive index, and because of that it is also known as refracted light. This refracted light in its term hits the inside surface of the particle and the phenomenon repeats, some light is reflected and another part is transmitted/refracted, and the cycle continuous, this time for the interior reflected light, until the light extinguish. The light that comes from the refraction of the internal surface is known by 1st order refraction (see fig.2.6) [7].

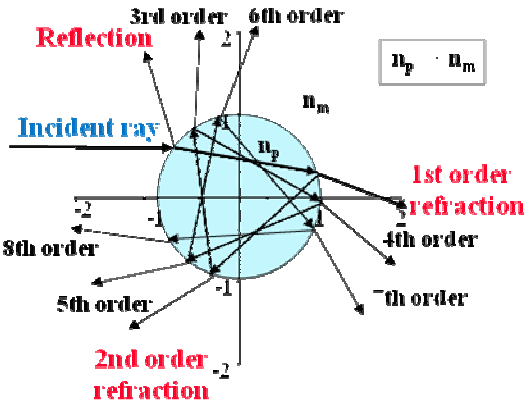

Figure 2.5- Scattered light in a droplet

As different rays light enter with different angles into the sphere they will follow different optical paths and this generates a phase shift between (two) different light rays. If we measure the phase shift of the reflected or the 1st refracted light, that are receiver by the detectors we can correlate the particle size (the diameter of the sphere) with the phase

shift. The correlation for the refracted light can be traduced by the Eq.(2.12)and Eq.(2.13) [8].

$$\Phi_{reflection} = \frac{2\pi d_p}{\lambda} \frac{\sin\theta \sin\psi}{\sqrt{2(1-\cos\theta\cos\psi\cos\varphi)}} \quad \text{(Eq.2.12)}$$

$$\Phi_{refraction} = \frac{2\pi d_p}{\lambda} \frac{n_{rel}\sin\theta\sin\psi}{\sqrt{2(1-\cos\theta\cos\psi\cos\varphi)(1+n_{rel}^2 - n_{rel}\sqrt{2(1+\cos\theta\cos\psi\cos\varphi)})}} \quad \text{(Eq.2.13)}$$

The size signal is a sinusoidal function and therefore the phase shift used to measure the particle size cannot exceed 2π (see fig.2.7)

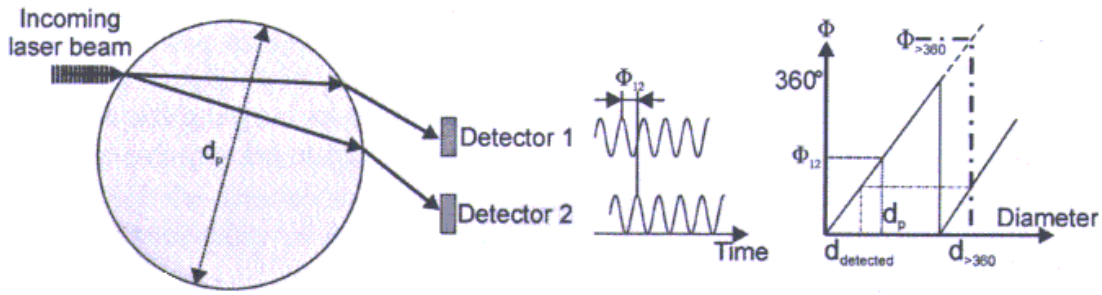

Figure 2.6- Size measuring with a two detectors system

As the phase differences increases with the particle size, for particles with a big size the phase difference can exceed 2π and in this case they will be detected as small particles, if we use two detectors.

A three-detector set-up can solve this problem by comparing the receiver signal from the three separated detectors (see fig. 2.7).

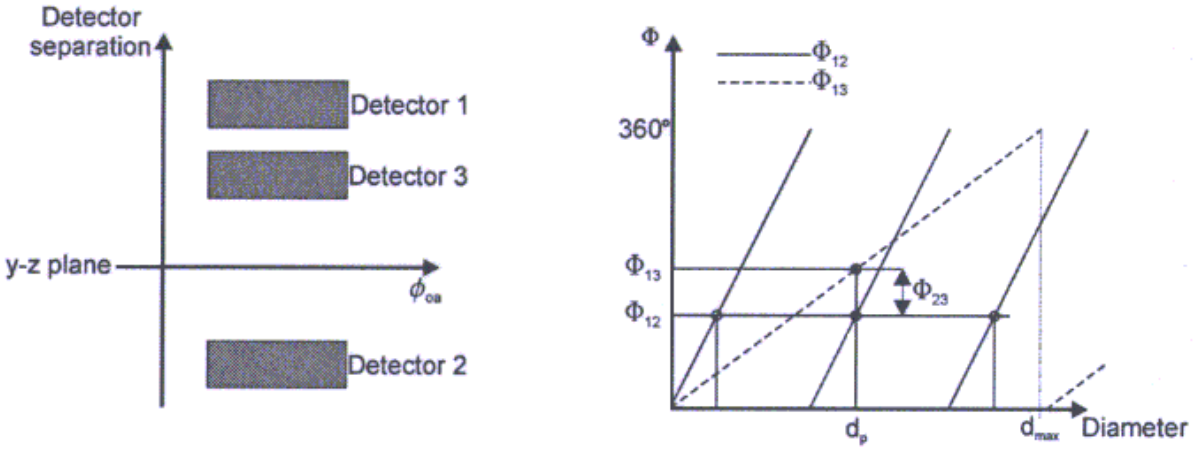

Figure 2. 7 - Determination of the particle size using a 3 detectors system

In fig.2.8 is represented a graphic with droplet size for different Pressures and positions in the spray resulting from a Spray injection measurement with a PDA system [courtesy P. Dahlander].

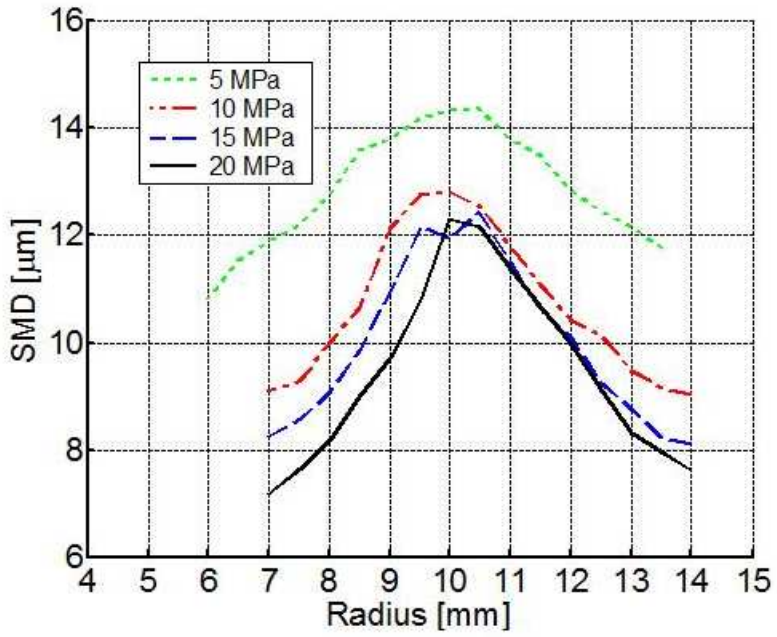

Figure2.8 - Plot of the droplet size (Saut medium Diameter) for a fuel injection spray obtained by a PDA system.

2.2.3. Advantages

- A non-intrusive measurement – the analyzing system does not interfere with the measuring object, and so does not influence the measuring results.
- An absolute measuring technique – this has as big advantage the necessity of the system calibration.

- A very high accuracy and high spatial resolution- mainly because of the high light frequency and the small probe volume.

2.2.4. Disadvantages

- A single point measuring method – as just one point and one particle in space can be measure at a time this is a very time consuming technique and we cannot get the instantaneous spatial flow structure.
- In certain applications, e.g. to measure velocity in continuous phase flows, seeding particles must be added, and these should be well chosen in order to well characterize the velocities field in the flow.

2.2.5. Preconditions

- Optical access to the measuring region
- Sphericity of the particles – if the droplets in the flow are not spherical but for example elliptical this will lead to an oversize/undersize, depending on its orientation, of the dimension, that can be as bigger as the difference between the shapes was.
- Particle sizes between 0.5 µm to several mm- The exact diameter that can be detected are dependent on the systems configuration. The upper limit of the system's measurement range is defined by the beam waist of the measuring volume (and normally the particle size should not exceed 1/3 to 1/2 of the beam waist diameter.)
- Limited particle Density – a very dense medium leads to more than one particle in the measuring volume at the same time, it also causes too much dispersion of the light that in one way decreases the important signal received and in another way it will increase the noise due to the multiple scattering.
- Refractive Index – to be able to measure the particle size with a PDA, the relative refractive index between the droplet and the surrounding medium should be known. In the specific case of the Fuel Injection Research this could be a problem when characterizing evaporation spays, as the droplets are submitted to different conditions of pressure and temperature and this leads to different values for the refractive index [9].

2.2.6. Applications

The PDA system is an optical device of measuring with huge fields of application as:

- **Power production** and that includes: Liquid metal atomization, Spray drying, etc.
- **Bubble dynamics**, and that includes: multiphase mass transfer
- **Spray and liquid atomization processes** as pharmaceutical sprays, paint coating, water sprays, and the most important for us **Fuel Injection**.

2.3. Direct Injected Gasoline Engines

The Direct injection (DI) is a post-mixture procedure/mode alternative to the pre-mixture system known as Port Fuel Injection (PFI), and very traditional in Gasoline automotive engines. In traditional PFI the fuel is injected onto the intake of the cylinder head and mixes with the air before enter into the cylinder. In opposite for DI the fuel is directly introduced in the cylinder (combustion chamber) where it evaporates and mixes with the air.

The usage of DI instead of the traditional PFI presents some advantages as fuel consumption reductions (no need to create and maintain a fuel film in the intake pipe) and more quick transient response (fun to drive) but also an increase of the cycle efficiency.

As the heat used in the evaporation of the fuel is taken from the surroundings, the temperature inside the cylinder will decrease and this reduces the engine's sensitivity to knock that is one of the biggest limitations for Gasoline engines, and thereby permits to increase the compression ratio, which leads to a higher Cycle efficiency.

The DI is divided into to two types of operational modes, the Direct Injection Stratified Charge (DISC), used at low to moderate engine load and speed, and the Homogeneous Charge Compressed Ignition (HCCI) used for moderate engine loads and speeds [10].

2.3.1. Direct Injected Stratified Charge

In DISC the fuel is inject in a restrict region of the cylinder, creating a combustible mixture in a limited region of the combustion chamber, surrounded by an insulation layer of a non-combustible mixture of air or residual gases. This insulation layer reduces the heat external losses and as the need for throttling is diminished also the pumping losses [11].

This mode represents a great opportunity to reduce the CO_2 emissions and fuel consumption.

However its potential it still a field under developed once to create a restrict mixture region demands a great knowledge about the injection systems.

2.3.2. Homogeneous Charge Compression Ignition

HCCI is a process of self-ignition (and spontaneous combustion) that is mainly controlled by the uniformity of the air/fuel mixture and by the chemical kinetics (charge temperature) [11].

The HCCI mode also presents a great potential to increase the fuel conversion efficiency and also reduce the NO_x emissions, however it also present by now some limitations as: a small operational window in terms of speed and load, a difficult control of the start of combustion, amoung others.

Although its potential, achieving an efficient DI system requires a great knowledge about the injection systems, that includes the spray distribution and atomization. That implies among other things to measure the droplet sizes in order to modulate the spray or simply to study the mixture.

2.4. Fuels

The liquids studied in this work are the typical fuels used in Direct Injection engines with exception of Diesel, and Isooctane. They can be divided into two main groups the multi-components, where are included Gasoline, E85, E95, MCF1 and Diesel, and The single components where is included the Isooctane, and also could be included E95 because it is almost a pure liquid.

The refractive index of all components with exception of Diesel and MCF1 were study under the influence of pressure and temperature, separately, with the main objective of evaluate their usage with PDA measurements.

2.4.1 Multi-components

In tables 2.1 to 2.5 are presented the main type of components and also the typical percentage range of its usage.

- **Gasoline:** The gasoline composition depends on many factors, as the country, the company, the region of the country or even the season of the year. This makes difficult to characterize the composition of Gasoline, and the same is true for Diesel. However each country has his one legislation where is establish the standard

components and their limits. The tables 2.1 and 2.5 are according to the Swedish Standards [12], [13], that are based on the European Community directives.

To overtop the problem of composition change on the experimental work we used Volvo Certificate Gasoline, which is also used in the others experimental researches in Chalmers Combustion Laboratory.

Alkanes	Aromatic molecules	Others	Boiling Point
60-70%	25-35%	5-10%	30-200°C

Table 2.1- Typical Gasoline Composition

- **E85:**The composition of E85 is based on [14]and is presented in tab.2.2

  E85 is a fuel with a high latent heat and so with a great potential to increase the DI Engines efficiency, because of the reasons presented in 2.3 and specially if combined with supercharging/Turbo charging DI [11]. These reasons emphasize even more the interest of study E85.

Ethanol	Gasoline	Benzene	N-hexane	Boiling Point
70-90%	10-20%	> 0.1%	> 0.2%	25-220°C

Table 2.2 – E85 composition

- **E95:** The advantages presented for E85 are also valid for E95

Ethanol	Residuals (mainly water)	Boiling Point
95%	5%	≈80-100°C

Table2.3 - E95 Composition

- **MCF1:** Multi-Component Fuel version 1 is a model fuel specially conceived for optical measuring work, especially for Laser induced fluorescence. It is composed mainly by Alkanes, which do not absorb light at typical laser wavelengths such as 266 and 355 nm, and they are also major components of Gasoline (and so it approximates the gasoline proprieties). Its composition is well defined and is presented in tab. 2.4.

The refractive index of MCF1 was just study under the influence of Temperature once it was not available at the time of the pressure studies.

Isopentane	Cyclopentane	Isooctane	Cyclootane	Decalin	Boiling Point
15%	15%	45%	18%	7%	28-175°C

Table2.4 -MCF1 Composition

- **Diesel**: The only objective of include this fuel in the studies was to determine its refractive index for the standard conditions of pressure and temperature. The same could also be made using a typical Refractometer as the Abbé refractometer.

AlKanes	Aromatic molecules	Others	Boiling Point
90-95%	10-5%	>5%	180-300°C

Table2.5 - Diesel Composition

2.4.2 Single Components

- **Isooctane:** The isooctane is a single component fuel that has been used to characterize spray behavior using a PDA system. Therefore, the evaluation of the variations on its refractive index depending on pressure and temperature is important to evaluate the accuracy of the previous studies.

Designation	Main constitution (% by weight)	Boiling Point
C8 H18	84C, 16H	99°C

Table 2.6- Isooctane Composition

2.4.3. Liquids and the Refractive Index

On tab.2.7 are presented the refractive index of some organic components that are typical included in the composition of the liquids presented. They are divided in tree main groups the Alcohols, the Alkanes also known as Paraffins and the Aromatic Moleculs. Connected to Alkanes but with a slightly different structure are the Cyclo-Alkanes.

The values presented in tab.2.7 are according with the information given by [15] and are relative to a wavelength of 589 nm.

	Molecular Formula	$T_{boiling}$ (^oC)	T_{ref} (^oC)	n
Alcohols				
Butanol	$C_4H_{10}O$	117,73	20	1,3988
Ethanol	C_2H_6O	78,29	20	1,3611
Methanol	CH_4	64,60	20	1,3288
Paraffins-Alkanes				
Isopentane	C_5H_{12}	27,88	20	1,3537
Pentane	C_5H_{12}	36,06	20	1,3575
Isooctane	C_8H_{18}	99,22	25	1,3884
Octane	C_8H_{18}	125,67	25	1,3994
Decane	$C_{10}H_{22}$	174,15	25	1,4090
Cyclo Alcanes				
Cyclopentane	C_5H_{10}	49,30	20	1,4065
Cyclooctane	C_5H_{11}	149,00	20	1,4586
Cyclodecane	C_5H_{12}	202,00	20	1,4716
Aromatic Molecules				
Cumene	$C_{12}H_{18}$	204	20	1,4915
Diisopropylbenzene	C_9H_{12}	152,41	20	1,4960
Toluen	C_7H_8	110,63	25	1,4941
Benzene	C_6H_6	80,09	20	1,5011

Table 2.7- refractive index of Organic Components

From the visualization of graf.2.1 stick out four main lines that represent the different groups of organic molecules that have been presented. From the graphic it is clear to see that the Aromatic Molecules are the ones with most high refractive index, followed by the Cyclo-Alkanes (the values presented in graf. 2.1 are according to tab 2.7).

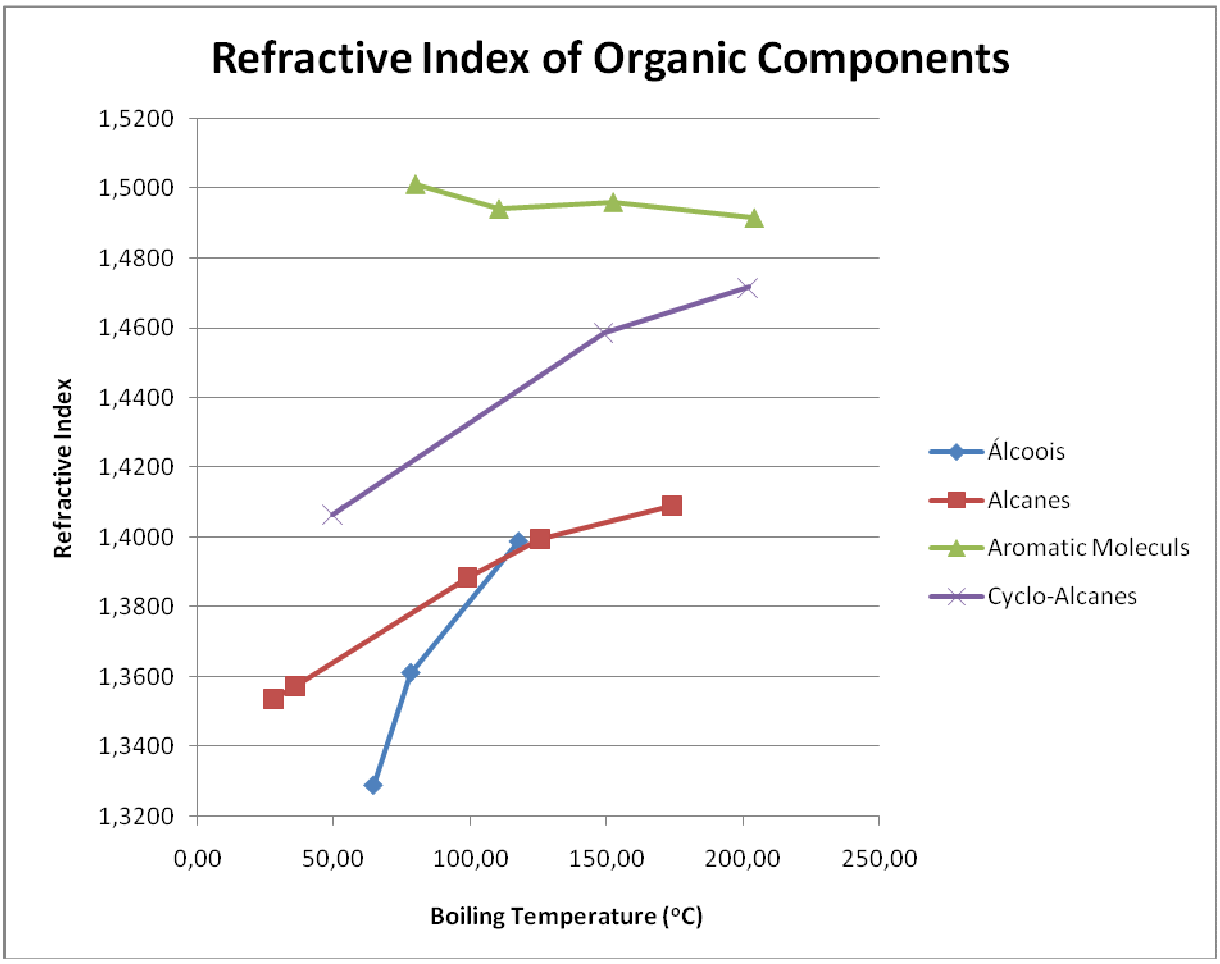

Graphic 2.1-Refractive Index from organic molecules relatively to their boiling point.

The temperature derivative of the refractive index for Ethanol is presented in tab.2.8, although is not available for the wavelength used in the experimental work, its values might be of great utility to compare with experimental results E95, as it seems not to be much affected by the wavelength, is not relevant at list if we were just interested in the first unit.

Ethanol			
λ (nm)	T (K)	$dn/dT \times 10^4$ (K^{-1})	Ref.
546.07	298	-4.05	16
600.00	278-298	-4.38	17
632.80	298	-4.00	16

Table2.8- Temperature derivative of the refractive index for methanol

As E95 can be consider as almost pure the influence of the composition change would not affect so much the results comparison.

3. Experimental work

The Experimental work is composed by two parts

- **Experimental work 1**: This experimental work was designed and carried out with the objective of measuring the absolute value of the refractive index for different liquids (Isooctane, E85, E95, Gasoline, Diesel, Methanol, Isobutanol, and Butanol) and for the same wavelength used in PDA measurements, more precisely green light (λ=514nm). The conditions of pressure and temperature were the environmental ones, i.e. room temperature (T=25^{o}C) and atmospheric pressure. In this experimental work the evolution of the n with temperature for one single component (Isooctane) and one multi-component (Gasoline) was also studied, but these results will be presented together with Exp. 2 results. The desired accuracy for the refractive index measurements was better than 0.01.

- **Experimental work 2**: This experimental work was carried out in Chalmers 4w HP/HT Spray Rig, with the objective of studied the evolution/dependence of the *n* with temperature and pressure (the range of values for temperature and pressure include the engine usage, ΔT=0-80^{o}C, ΔP=0-30bar), a simultaneous study of pressure and temperature would be also of big interest, but unfortunately due to lack of time it was not possible to complete within this project. The value of refractive index *n* was measured by comparing with substances with a known n, and so we can call it a relative measuring/method. The *n*(T) and *n*(P) evolution were studied for Isooctane, Gasoline, E85, E95, and MCF1, the reference fluids were Methanol, Fluorobenzene and Butanol.

- **Experimental work 3**: In this experimental work we attempt to estimate and analyze the evolution of the refractive index with the composition change; This was not initially included in the project plans, but after performing the *n*(T) study it was found of great importance to first of all evaluate the isolated effect of the temperature and second of all to achieve a generic understanding about the major effects of the composition on the refractive index. To perform this experimental work no special setup was designed. The liquids measured were gasoline and MCF1 manly because among all multi-components studied they are the ones most affected by the composition change.

Although we present the experimental work by this order this does not correspond to the order used to carry out the experience, Because of the schedule for the chamber usage, the presented Exp.2 was carried in first place, witch by somehow had limited our work.

3.1. Experimental work 1

3.1.1. Equipment

The equipment used for the first setup was: a Laser, a Refraction Cell, some optical accessories, and a ruler.

- **Laser**

Figure 3.1-Laser light source

The Laser emitter used (see fig.3.1) was the PDA laser source, 2D TSI/Aerometric PDPA-system. It is an Argon Laser (the gain medium is an ionized Argon) emitting in the wavelength range of blue-green light ($\Delta\lambda$=488-514nm) with continuous emission and a diameter beam of approximately 5 mm.

Figure 3.2 - Refraction Cell

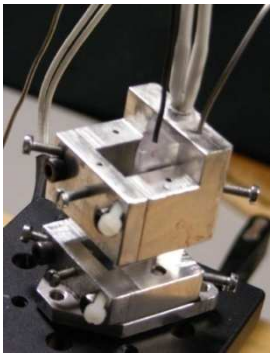

- **Refraction Cell**

The Refraction Cell (fig.3.2) is a special device design for this project to contain the measured liquid. This device should also fulfill with the specifications of the experimental work, i.e. be able to change the temperature of the liquid, allow optical access for 3 surfaces, have the right dimensions in order to fit into the chamber, and finally have the enough stability to assure a fixed position (for all components). Its main function is to heal the liquid to be measure. It is composed by:

1. Metallic Body: An aluminum block with a rectangular hole for cuvettes and prism with apertures in its faces, in order to allow light to cross through. The rectangular shape was chosen in order to allow also the usage of two cuvettes at the same time.

2. Cuvette- Hellma QS: Triangular Hollow Optic Prism made by suprasil quartz, with 2x45^{o} angles. Dimensions: 2 x (a=12.4 mm), l = 45 mm.

3. Cartage heater- Backer C: cylindrical heater with 6.5 mm diameter, 38 mm length and 150 watts.

4. Thermocouple type K

5. Temperature controller: device used to control the heating power, by comparing the stated temperature with the readied temperature by the thermocouple.

- **Optical Accessories**

  Some optical accessories were used to guide and filter the light from the Laser emitter to the refraction cell, more precisely two 90^{o} prisms and a filter.

  1. 90^{o} prisms: is a quartz triangular prism that deflects the light 90^{o}.
  2. Blue light Filter: a filter that blocks the wavelength correspondent to blue, i.e. $\lambda \approx 488$ nm.

- **Ruler**

  Used as a ruler was a flat vertical platform /surface to which was added a strip of milimetric paper, where the points were marked.

3.1.2. Setup

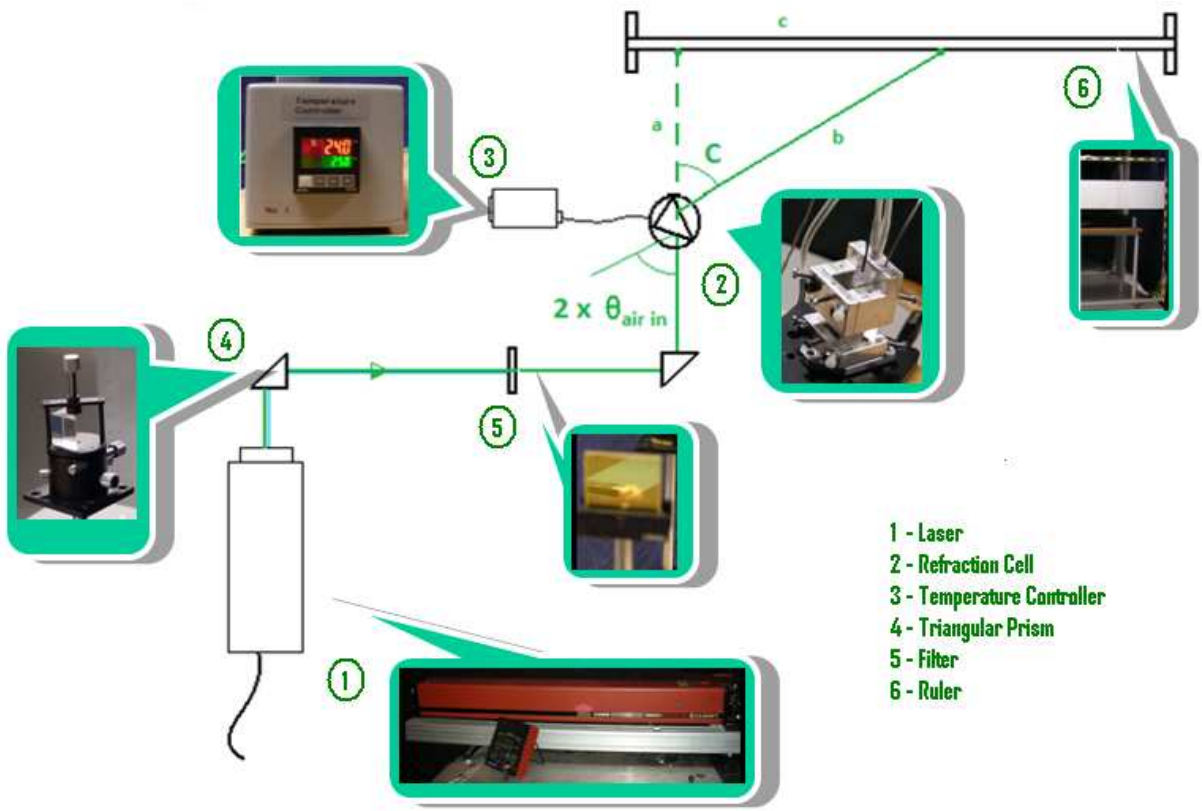

Figure 3.3-Setup of Experimental work 1

3.1.3. Description

The emitted light ($\Delta\lambda$=488-514 nm) coming from the laser (1) is 90^{o} deflected by a prism (2) and passes through a filter (5) that blocks the blue light, after it passes again through a triangular prism (4) that redirected the light to the refraction cell (2). The liquid inside the refraction cell refracted the light that comes through according to its refractive index, and finally the refracted light hits a ruler (6) positioned approximately 2.5m further away, where the spot is marked. By changing the liquid and the temperature inside the cuvette the diffraction angle of outgoing light will change and we can associate this to *n* change. Using the temperature controller (3) we can establish the temperature for the liquid (the temperature sated should be bigger or at least equal to the room temperature, as we do not dispose of a cooling system). Although we could read the temperature in the temperature controller, this was slightly differing from the temperature inside the liquid (since the thermocouple of the refraction cell is positioned in the metal body), the option was to use an extra Thermocouple insert in the liquid.

3.1.4. Measuring

To measure the refractive index of the liquid using this setup, we should measure the incoming and outgoing angles of the light (related to the normal surface of the cuvette) on the refraction cell, as shown in fig 3.4.

To measure the incoming angle we make use of the back reflection of the incoming light. The intersection of a chosen plane with back reflection defines a point, if we consider the other two points resulting from Prism light intersection and the incoming point in the cuvette we can defined a triangle with a know distances that we can use to calculate the angle between the incoming (incident) and back reflected light, by applying the Cosines Law. This angle is two times bigger than the incoming angle relative to the normal surface that we are interested in measure.

To measure the outgoing angle, that for this method should be larger than 45^{o}, we define an additional angle, C. This is the angle between the outgoing light with a empty cuvette (and that means parallel to the incoming light, as the influence of the cuvette walls can be neglected) and a filled cuvette (with the liquid we want to study), once again this angle can be calculated by measuring the distances between the points and applying an adapted version of the Cosines law. Looking at Fig.3.5 we can get a better perception about the description.

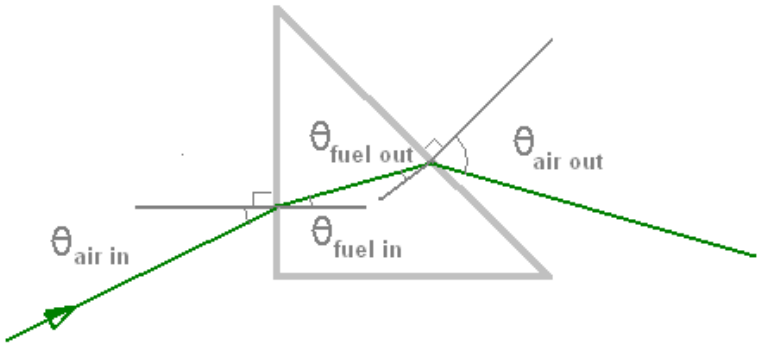

Figure 3.4- characteristic angles of the cuvette

For each set of measurements of $\theta_{air\ out}$ (outgoing angle for air), the $\theta_{air\ in}$ (incoming angle from air) was fixed. The Eq.3.1 and Eq.3.2 were used to calculate $\theta_{air\ in}$ and $\theta_{air\ out}$. The referred angles are represented in fig.3.4.

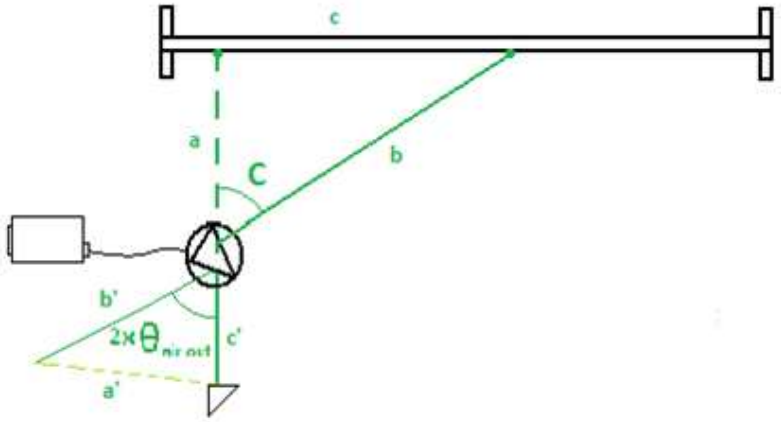

Figure3.5-schequeme of the Angles measuring

$$\theta_{\text{air in}} = \frac{\arccos\left(\frac{b'^2+c'^2-a'^2}{2\,b'\,c'}\right)}{2} \qquad \text{(Eq.3.1)}$$

$$\theta_{\text{air out}} = \frac{\pi}{4} - \theta_{air\ in} + ar\cos\left(\frac{b^2+a^2-c^2}{2\,b\,a}\right) \qquad \text{(Eq.3.2)}$$

Finally using $\theta_{air\ in}$ and $\theta_{air\ out}$ we can calculate the refractive index of the sample, using the Eq. 3.3.

$$n_{\text{liq}} = \frac{n_{\text{air}}\sin\theta_{\text{air out}}}{\sin\left(\frac{\pi}{4} - \arcsin\left(\frac{n_{\text{air}}\sin\theta_{\text{air in}}}{n_{\text{liq.}}}\right)\right)} \qquad \text{(Eq.3.3)}$$

In the particular case of $\theta_{air\ in}$ being 0^o this formula can be simplified, which would not apply any longer for an iterative process.

3.1.5. Experimental Results

1st set of measurements

For the first set of measurements the incoming angle was, $\theta_{air\ in} = 0^o \pm 0.1^o$ and the results for the refractive index are listed in table 3.1. In this table u_θ and u_n represents the uncertainty associated with the θ and *n* calculations, the details of their calculation will be presented in uncertainty analysis.

Substance	Temperature (° C)	$\theta_{air\ out}$	u_θ	n	u_n
Methanol	25.7	69.81°	0.14°	1.327	0.001
Isobutanol	25.7	79.46°	0.17°	1.390	0.001
E 85	25.6	74.30°	0.16°	1.362	0.001

Table 3.1-Results of the refractive index for an incoming angle of 0^o

2nd set of measurements

To be able to measure the full range of values for the refractive index, i.e. to be able to measure bigger refractive index the incoming angle was increased and this leads to a reduction of the outgoing angle. So for this set of measurements (tab.3.2) the calibrated angle used was $\theta_{air\ in} = 32.16^o \pm 0.25^o$.

The repetition of measurement of the same liquids for different angles is also a helpful way to analyze the validity of the results obtained.

Substance	Temperature (° C)	$\theta_{air\ out}$	u_θ	n	u_n
E 95	26.2	30.60°	0.26°	1.360	0.01
E 85	26.3	30.89°	0.26°	1.366	0.01
Isooctane	26.4	31.04°	0.27°	1.369	0,01
MCF 1	26.2	32.01°	0.27°	1.388	0.01
Gasoline	26.2	34.41°	0.27°	1.434	0.01
Isobutanol	26.2	32.35°	0.26°	1.395	0.01
Butanol	26.0	31.54°	0.27°	1.378	0.01
Diesel	26.4	35.09°	0.27°	1.446	0.01
Methanol	26.4	28.88°	0.26°	1.326	0.01

Table 9- Results of the refractive index for an incoming angle of 32.16^o

3nd set of measurements

The third set of measurements was for study the evolution of *n* with temperature, for Isooctane and Gasoline, although we present here the results the analysis of them will be held for later discussion, i.e. together with the same measurements for n(T) on the 2nd experimental work.

The calibrated angle used in this set of measurements was, $\theta_{air\ in}=31.76^{o} \pm 0.22^{o}$. The explanation for not using the same angle as in 2sd set of measurements is a repositioning and recalibration of the system compared to the previous measurements.

Substance	Temperature (° C)	$\theta_{air\ out}$	u_θ	n	u_n
Diesel	27.1	35.61°	0.23°	1.448	0.01
Gasoline	27.2	34.55°	0.23°	1.429	0.01
Gasoline	40.1	34.23°	0.23°	1.422	0.01
Gasoline	58.6	33.88°	0.23°	1.415	0.01
Gasoline	77.1	33.73°	0.23°	1.413	0.01
Gasoline	33.9	35.04°	0.23°	1.438	0.01
Isooctane	30.9	32.57°	0.23°	1.389	0.01
Isooctane	40.2	32.32°	0.23°	1.386	0.01
Isooctane	59.2	32.73°	0.23°	1.376	0.01
Isooctane	78.1	31.37	0.23°	1.367	0.01

Table 3.3- Results of the refractive index for an incoming angle of 31.76°

From the comparison of different results, and that includes the crossed measures and the values found in literature and presented in this thesis, we can confirm the results obtained, and we can even notice that normally the difference between the comparison lead to an error that is less than the estimated U_n. The only exception seen was the value measured for Isooctane in the second set of measurements, which is contradicting all the values measured and found in the literature. This might had happen because of a non-expected variable, as for example some contaminant in the cuvette or a miss spell when noting the measured distance, and so this value should not be considered.

3.1.6. Uncertainty Analyses

The previous values presented four u_θ and u_n were based on the calculated uncertainty analyses.

The uncertainty analyses is also a complex issue to by evaluated due to the many sources of errors/uncontrolled variables, and because of that requires some simplifications, this is also a issue that is related to the experience of the experimentalist.

The main sources of errors are concerning the distance and Temperature measurements, dividing the errors in systematic and random errors, we can detail them as:

- Systematic errors:

  - Distance measuring: this error was estimated in 0.25% of the measured distance

  - Thermocouple calibration: the thermocouple was calibrated using a Pt_{100} as a reference, and its calibration curve is presented in Appendix 1 (tab.1.a and graphic 1.a). The Pt100 was calibrated by a laboratory and has an uncertainty of 0.1°C. The maximum uncertainty for our thermocouple is 0.7°C. These thermocouple was also used to measured the temperature of the liquids for the others experimental works.

  Random errors:

  - Scale resolution of the ruler: 0.5 mm

  - Scale resolution of the digital temperature converter from the thermocouple.

The other sources of errors can be neglected due to their minimum influence on the accuracy of the measurements.

The Uncertainty Analyses that is presented follows the methodology presented by Hugh W. Coleman [18].

The random contribution (B_θ) for U_θ is given by Eq.3.4, is calculated from b_{xi}, where s represents the standard deviation (half of the minimum value of the scale) and k is the constant that allows to extend the final standard deviation to 95% of confidence level. To obtain the value of k, we consider a uniform distribution for the ruler resolution.

$$s = \frac{a}{\sqrt{3}} = 0.29\,\text{mm} \qquad b_{x_i} = s \cdot k = 0.29 \times 1.65 = 0.48\,mm$$

$$B_\theta = \sqrt{\sum_{i=1}^{n} \left(\frac{\partial \theta}{\partial x_i} \cdot b_{x_i} \right)^2} \qquad \text{(Eq.3.4)}$$

The systematic contribution due to measure distances x_i (P_θ) are represented by Eq.3.6

$$p_{x_i} = 0.0025 \cdot x_i$$

$$P_\theta = \sqrt{\sum_{i=1}^{n}\left(\frac{\partial\theta}{\partial x_i}\cdot u_{x_i}\right)^2} \qquad \text{(Eq.3.6)}$$

The total value of U_θ is obtained by combined the effect of the random and systematic errors (Eq.3.7). The covariance between the distance measured (a', b', c', a, b and c) were neglected.

$$U_\theta = \sqrt{B_\theta^2 + P_\theta^2} \qquad \text{(Eq.3.7)}$$

$$\theta \pm U_\theta$$

For $\theta_{air\ in}$

$$\frac{\partial\theta_{air\,\mathrm{in}}}{\partial \mathrm{a}'} = \frac{1}{2}\cdot\frac{1}{\sqrt{1-\left(\frac{a'}{2b'}\right)^2}}\cdot\frac{1}{2b'} \qquad \text{(Eq.3.8)}$$

$$\frac{\partial\theta_{air\,\mathrm{in}}}{\partial \mathrm{b}'} = -\frac{1}{2}\cdot\frac{1}{\sqrt{1-\left(\frac{a'}{2b'}\right)^2}}\cdot\frac{a'}{2b'^2} \qquad \text{(Eq.3.9)}$$

For the others angles

$$\frac{\partial\theta_{air\,\mathrm{in}}}{\partial \mathrm{a}'} = \frac{1}{2}\cdot\frac{1}{\sqrt{1-\left(\frac{b'^2+c'^2-a'^2}{2b'c'}\right)^2}}\cdot\frac{a'}{b'c'} \qquad \text{(Eq.3.10)}$$

$$\frac{\partial\theta_{air\,\mathrm{in}}}{\partial \mathrm{b}'} = -\frac{1}{2}\cdot\frac{1}{\sqrt{1-\left(\frac{b'^2+c'^2-a'^2}{2b'c'}\right)^2}}\cdot\frac{4b'^2c'-2c'(b'^2+c'^2-a'^2)}{(2b'c')^2} \qquad \text{(Eq.3.11)}$$

$$\frac{\partial\theta_{air\,\mathrm{in}}}{\partial \mathrm{c}'} = -\frac{1}{2}\cdot\frac{1}{\sqrt{1-\left(\frac{b'^2+c'^2-a'^2}{2b'c'}\right)^2}}\cdot\frac{4b'c'^2-2b'(b'^2+c'^2-a'^2)}{(2b'c')^2} \qquad \text{(Eq.3.12)}$$

The main difference between the first angle and the other is the equation that was used to calculate the $\theta_{air\ in}$.

For $\theta_{air\ out}$ the $d\theta/dx_i$ are:

$$\frac{\partial \theta_{air\,\mathrm{in}}}{\partial \mathrm{a}} = -\frac{1}{\sqrt{1-\left(\frac{b^2+a^2-c^2}{2\,b\,a}\right)^2}} \cdot \frac{4b^2a - 2\,b\,(b^2+a^2-b^2)}{(2\,b\,a)^2} \qquad \text{(Eq.3.13)}$$

$$\frac{\partial \theta_{air\,\mathrm{in}}}{\partial \mathrm{b}} = -\frac{1}{\sqrt{1-\left(\frac{b^2+a^2-c^2}{2\,b\,a}\right)^2}} \cdot \frac{4b\,a^2 - 2\,a\,(b^2+a^2-b^2)}{(2\,b\,a)^2} \qquad \text{(Eq.3.14)}$$

$$\frac{\partial \theta_{air\,\mathrm{in}}}{\partial \mathrm{c}} = \frac{1}{\sqrt{1-\left(\frac{b^2+a^2-c^2}{2\,b\,a}\right)^2}} \cdot \frac{c}{b\,a} \qquad \text{(Eq.3.15)}$$

$$\frac{\partial \theta_{air\,out}}{\partial \theta_{\mathrm{air\,in}}} = -1$$

To calculate the uncertainty of the *n*, we consider all sources of errors as fossilized, and so their contribution appears as a systematic error.

$$n = \frac{n_{air}\,\sin\theta_{air\,out}}{\sin\theta_{\mathrm{fuel\,out}}} \qquad \text{(Eq.3.16)}$$

The influence of n_{air} can be neglected, as it just changes after the 3rd decimal place, and our measurements are just with three decimal places, and so the calculation of U_n is resumed to:

$$U_n = \sqrt{\left(\frac{\partial n}{\partial \theta_{air\,\mathrm{out}}} \cdot u_{\theta_{air\,out}}\right)^2 + \left(\frac{\partial n}{\partial \theta_{fuel\,\mathrm{out}}} \cdot u_{\theta_{fuel\,out}}\right)^2} \qquad \text{(Eq.3.17)}$$

$$\frac{\partial n}{\partial \theta_{air\,out}} = \frac{\cos\theta_{air\,\mathrm{out}}}{\sin\theta_{\mathrm{fuel\,out}}} \qquad \text{(Eq.3.18)}$$

$$\frac{\partial n}{\partial \theta_{\mathrm{fuel}\ out}} = \frac{\cos\theta_{air\,\mathrm{out}} \cdot \sin\theta_{fuel\,out} - \sin\theta_{air\,\mathrm{out}} \cdot \cos\theta_{fuel\,out}}{\sin^2\theta_{fuel\,out}} \qquad \text{(Eq.3.19)}$$

The calculation of u is also a iterative process

$$U_{\theta_{fuel\,out}} = \sqrt{\left(\frac{\partial \theta_{fuel\,out}}{\partial \theta_{air\,in}} \cdot u_{\theta_{airin}}\right)^2 + \left(\frac{\partial \theta_{fuel\,out}}{\partial n} \cdot u_n\right)^2} \qquad \text{(Eq.3.20)}$$

As this last equation shows, not only the calculation of n is an iterative process as also the calculation of the errors.

$$\frac{\partial \theta_{fuel\,\mathrm{out}}}{\partial \theta_{\mathrm{air\,in}}} = \frac{1}{\sqrt{1-\left(\frac{\sin\theta_{air\,\mathrm{in}}}{\mathrm{n}}\right)^2}} \cdot \frac{\cos\theta_{air\,\mathrm{in}}}{\mathrm{n}} \qquad \text{(Eq.3.21)}$$

$$\frac{\partial \theta_{fuel\,\mathrm{out}}}{\partial n} = -\frac{1}{\sqrt{1-\left(\frac{\sin\theta_{air\,\mathrm{in}}}{\mathrm{n}}\right)^2}} \cdot \frac{\cos\theta_{air\,\mathrm{in}}}{\mathrm{n}^2} \qquad \text{(Eq.3.22)}$$

However to use this approach calculating the uncertainty for this experimental work is not very simple or convenient. To simplify the error analyses the dependence of the refractive index was reduced just to $\theta_{\mathrm{air\ out}}$. There is no big implications with this assumption, and mainly because from the crossed results of the different measurements we can note that the uncertainty was in the majority of the times overestimated, but even so to assure the validity of this simplification we pick one of the measurements (in this case it was the measurement of Methanol using an incoming angle of 32.1^{o}) and we calculate the uncertainty using the complete analyze, the difference obtained was from 0.01 (for the simplified version) to 0.012 (for the complete analyze).

$$U_n \cong \sqrt{\left(\frac{\partial n}{\partial \theta_{air\,\mathrm{out}}} \cdot u_{\theta_{air\,out}}\right)^2} \qquad \text{(Eq.3.23)}$$

3.2. Experimental work 2

This second experimental work can be divided in to two parts. In the first part we studied *n*(P) evolution meanwhile in the second part we studied the *n*(T) evolution.

3.2.1. Equipment

The equipment used for the first setup was: the Chalmers 4w HP/HT Spray Rig, a Laser, a Refraction Cell, some optical accessories, and a ruler.

- **Chalmers 4 windows High Pressure/High Temperature Spray Rig**

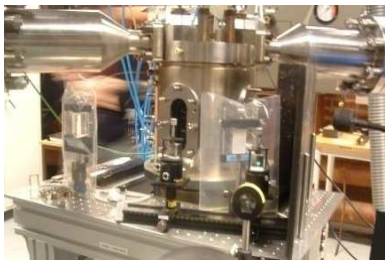

Figure3.6- Chalmers 4w HP/HT Spray Rig

The Chalmers High Pressure and High Temperature (HP/HT) spray rig is an optically accessed cylindrical chamber (Fig.3.8) capable to mimic the in-cylinder environment of an internal combustion engine (the maximum air pressure is 100 bar and the maximum air temperature is 600^{o}C), allowing optical access due to 4 quartz glass windows with 40 x 100 mm^{2}, placed symmetrically.

- **Laser**

Figure3.7- PDA Laser emitter

The laser used was the same one of Exp. Work 1 but instead of picking the light directly from the source we used the PDA emitter (Fig.3.7).

- **Refraction Cell**

Figure3 .8- Refraction Cell plus the adapter to the chamber

The refraction Cell (Fig.3.8) used was the same but we added an extra support to be able to connect it to the chamber. The support is composed by a metallic arm, where the Refraction Cell stands, connected to a metallic window that fits in one of the chamber windows.

- **Optical accessories**

In this setup were used two triangular prisms and a focus lens.

Restrictions

The usage of the Chalmers 4w HP/HT Spray Rig implies optical field restrictions, once it is a metallic shell with just 4 widows with 40 cm^2 that gives an optical usable angle relative to the center of 21.9^o (see Fig.3.9). In order to assure the usage viability of the 4w (four windows) chamber we should verified if the total angles, resulting from the incoming and outgoing light, for the range of *n* that we expect fuels to lea in, are compatible to the chamber angles.

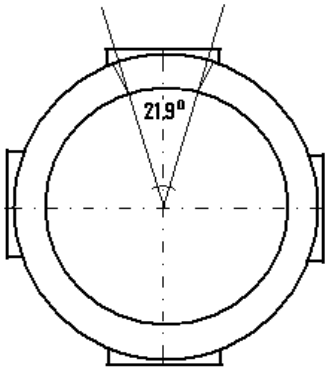

Figure 3.9- Center angle for the 4 windows bomb

Setting the extreme values for n of 1.3 and 1.5, and running a numerical case study using Excel, the results obtained are shown in table 3.4:

Table 3.4- Values of the resulting angles for different refractive index and incoming angles

***n* = 1.3**							***n* = 1.5**							**$\theta_{averege}$**	**180-θ_{avere}**	**$\theta_{aver.}$-θ_{Total}**
n	$\theta_{air\ nc.}$	$\theta_{fuel\ inc.}$	$\theta_{fuel\ out.}$	$\theta_{airout.}$	θ_{Total}	180-θ_{Total}	n	$\theta_{air\ nc.}$	$\theta_{fuel\ inc.}$	$\theta_{fuel\ out.}$	$\theta_{airout.}$	θ_{Total}	180-θ_{Total}			
1.3	10	7.7	37.3	52.0	163.0	17.0	1.5	10	6.6	38.4	68.6	146.4	33,6	154.7	25.3	8.3
1.3	12	9.2	35.8	49.5	163.5	16.5	1.5	12	8.0	37.,0	64.6	148.4	31,6	155,9	24.1	7.6
1.3	14	10.7	34.3	47.1	163.9	16.1	1.5	14	9.3	35.7	61.1	149.9	30,1	156.9	23.1	7.0
1.3	16	12.2	32.8	44.7	164.3	15.7	1.5	16	10.6	34.4	58.0	151.0	29,0	157.7	22.3	6.6
1.3	18	13.8	31.2	42.4	164.6	15.4	1.5	18	11.9	33.1	55.0	152.0	28,0	158.3	21.7	6.3
1.3	20	15.3	29.7	40.2	164.8	15.2	1.5	20	13.2	31.8	52.3	152.7	27,3	158.8	21.2	6.1
1.3	22	16.7	28.3	38.0	165.0	15.0	1.5	22	14.5	30.5	49.7	153.3	26,7	159.2	20.8	5.8
1.3	24	18.2	26.8	35.8	165.2	14.8	1.5	24	15.7	29.3	47.2	153.8	26,2	159.5	20.5	5.7
1.3	26	19.7	25.3	33.7	165.3	14.7	1.5	26	17.0	28.0	44.8	154.2	25,8	159.7	20.3	5.5
1.3	28	21.2	23.8	31.7	165.3	14.7	1.5	28	18.2	26.8	42.5	154.5	25,5	159.9	20.1	5.4
1.3	30	22.6	22.4	29.7	165.3	14.7	1.5	30	19.5	25.5	40.3	154.7	25,3	160.0	20.0	5.3
1.3	32	24.1	20.9	27.7	165.3	14.7	1.5	32	20.7	24.3	38.1	154.9	25,1	160.1	19.9	5.2
1.3	34	25.5	19.5	25.7	165.3	14.7	1.5	34	21.9	23.1	36.1	154.9	25,1	160.1	19.9	5.2
1.3	36	26.9	18.1	23.8	165.2	14.8	1.5	36	23.1	21.9	34.1	154.9	25,1	160.0	20.0	5.1
1.3	38	28.3	16.7	22.0	165.0	15.0	1.5	38	24.2	20.8	32.1	154.9	25,1	159.9	20.1	5.1
1.3	40	29.6	15.4	20.2	164.8	15.2	1.5	40	25.4	19.6	30.3	154.7	25,3	159.8	20.2	5.1
1.3	42	31.0	14.0	18.4	164.6	15.4	1.5	42	26.5	18.5	28.4	154.6	25,4	159.6	20.4	5.0
1.3	44	32.3	12.7	16.6	164.4	15.6	1.5	44	27.6	17.4	26.7	154.3	25,7	159.4	20.6	5.0
1.3	46	33.6	11.4	14.9	164.1	15.9	1.5	46	28.7	16.3	25.0	154.0	26,0	159.1	20.9	5.0
1.3	48	34.9	10.1	13.2	163.8	16.2	1.5	48	29.7	15.3	23.3	153.7	26,3	158.7	21.3	5.0
1.3	50	36.1	8.9	11.6	163.4	16.6	1.5	50	30.7	14.3	21.7	153.3	26,7	158.3	21.7	5.1

For the results shown in the table is easy to realize that for a refraction cell held in the center of the chamber the experimental work would not be doable (at least to these *n* extreme values). However the results shows the four windows (4w) are not adequate, and this is more suitable for 3w, once one of the angles between windows is 145°, the usage of 4w stills more desirable due to the advantage of having an extra window that can be used to fuel change, and also allows the usage of 2 cuvettes in the refraction cell (the total angle between the light for 2 cuvettes are near 180°).

To overcome this problem the refraction cell was displaced 18 mm from the center to border and with this instead of having a center angle between windows of 180° we have an angle of 161°, that allows to use the 4w chamber.

3.2.3. Setup

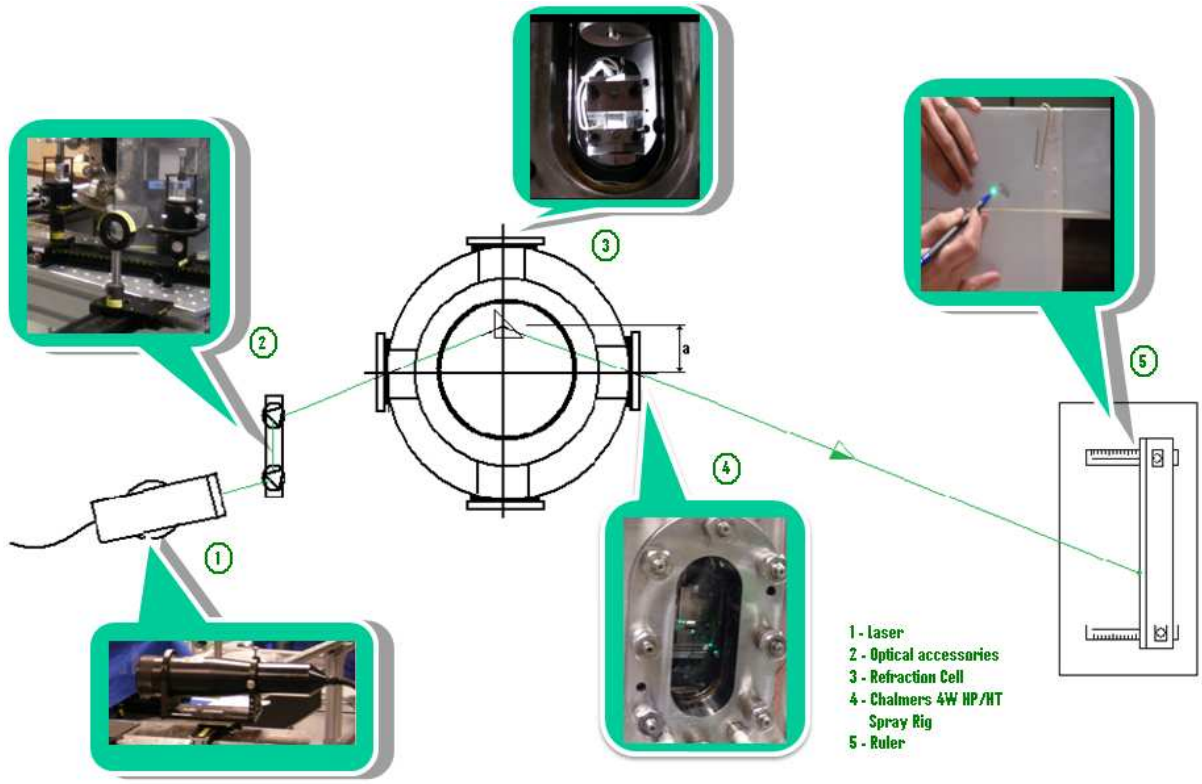

Figure 3.10- Setup for Experimental work 2

Description

The light coming from the PDA emitter (1) is focus and guided into the chamber (by the optical accessories), inside the chamber the light hits the liquid (inside the refraction cell) and is deflected, leading the light to get out of the chamber (by the opposite window) and heat the ruler (displaced approximately 2m far) where the point is marked. Once again, changing the liquid and its conditions (pressure and temperature) we change the outgoing angle (due to the variation on *n*) and that means the point on the ruler. The relation between the *n* and the position on the ruler is presented by Eq.3.24

$$x(n) = d\tan\left[\arcsin\left(n\sin\left(\frac{\pi}{4} - \arcsin\frac{k'}{n}\right)\right) - \frac{\pi}{4}\right] \quad \text{(Eq.3.24)}$$

$$k' = n_{air}\sin\theta_{air\,in} \quad \text{(Eq. 3.25)}$$

In this equation *d* represents the distance from the refraction cell to the ruler.

3.2.5. Relative Measure Method

By measuring the position of the points on the ruler (5) and knowing the relation of *x*(n) (or the inverse relation) as also the refractive index, *n* (for the same conditions used in the experience, i.e,. same temperature and it also should be the same wavelength), of some of the liquids used , we are able to calculate the absolute value of *n* from the different points. Although we can achieve the absolute values of *n* this is not what we are more interested in, but instead we are interested in the relative values of n (for the same substance and different conditions), i.e. the evolution of *n*(P) and *n*(T) (see fig.1.a in Appendix 1).

As this method does not apply for angles measuring to determinate *n* (and this is the big advantage), but only the relation to the refractive index of reference substances we can call it a Relative method.

3.2.5.1. Scale approximation.

Picking a value for $\theta_{air\ in}$ and represented a plot of Eq. 3.25 for different values of n we can verified that the curve trend almost as a straight line, as we can see in Graphic 3.1.

The value used for $\theta_{air\ in}$ was 14^{o} and this angle corresponds approximately to the incoming angle used in the experimental work, although we do not know this angle with enough accuracy (we did not measure it accurately) to be allowed to use Eq.3.24 as our measure

scale, it is enough to know if we can use as an approximation. Before any further conclusion we should check the influence of the deflection due to the quartz glass.

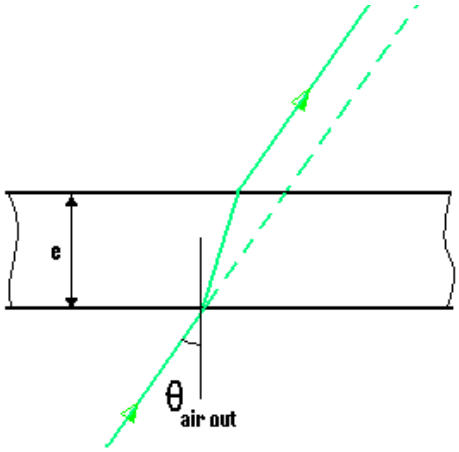

Figure 1011 - Deflection due to the quartz glass

$$x_{offset} = e \cdot \left[\sin\left(\theta_{air\_out} - \pi/4\right) - \sin\left[\arcsin\left(\frac{n_{air}}{n_{quartz}} \cdot \sin\left(\theta_{air\_out} - \pi/4\right)\right)\right]\right] \quad \text{(Eq.3.26)}$$

The expression showings the influence of the quartz glass (see fig.3.11) is expressed by Eq.3.26, and in Graphic. 3.1, we can see a plot of *x*(n) after taking the effect of the quartz glass out.

Graphic 3.1-Represantation of the x(n) and x(n) corrected

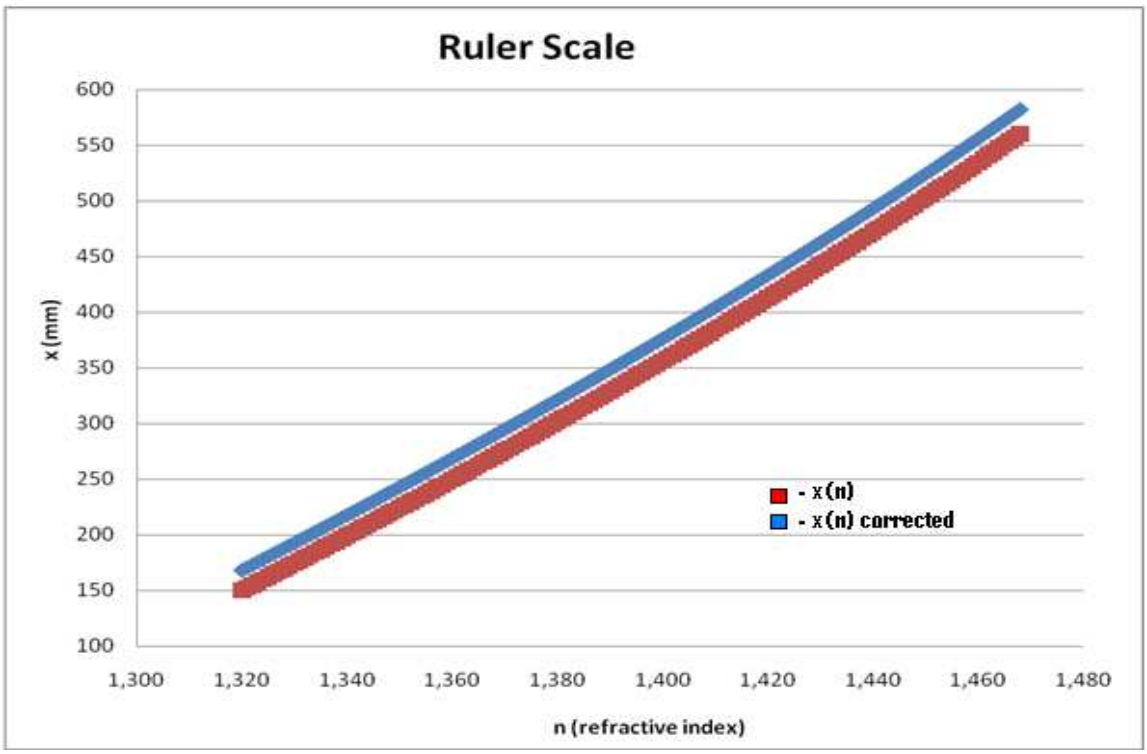

As was denoted for *x*(n) also *x*(n) corrected trends almost as a straight line, so if we pick two extreme points in the ruler, with a known refractive index, we can join this two points with a straight line that we can use as a scale for our ruler, and consider as a good approximation.

3.2.5.2. Reference Liquids

Substance	Mole. Form.	Mole. Weight	Boiling Temp.	Temperature	n (λ=589nm)
Methanol	CH_4O	32.04	64.6 °C	20 °C	1.3288
Butanol	$C_4H_{10}O$	74.12	117.7 °C	20 °C	1.3988
Fluorobenzene	C_6H_5F	96.10	84.73 °C	20 °C	1.4677

Table3.5-Proprities of the Reference Liquids

The liquids used as reference are presented in tab. 3.15, where is also presented the most relevant proprieties. These liquids were chosen based on their refractive index. Ethanol is from the typical components of the fuels the one that presents the lowest refractive index, in the odder extreme we have Fluorobenzene that in spite of not being a typical fuel component it has the biggest refractive index compare to the others; finally the Butanol is a component with a refractive index that is in the middle. As it is clear to notice, the values for *n* do not corresponds to the same λ used, one way to overcome this problem, once a different λ corresponds to a shift in all *n*, is by comparing the calculate values with this procedure with the values previously calculated. However we should remember that this procedure is just important if we are interested in present absolute values, which as it was said is not the case.

3.2.6. Pressure Study

3.2.6.1. Experimental Results

The ruler scale used for pressure study Methanol and Fluorobenzene as extreme reference values.

The symbol *n'* is used to refer to the refractive index calculated using the reference substances for the wavelength of 589 nm, and permits to distinguished from the *n*, commonly used in this thesis to refer to the refractive index, but in this particular case to refer to the 518 nm wavelength, also the symbols $*n'_{10bar}$ and $*n'_{30bar}$, were used in tab.3.7, 3.9, 3.11 and 3.13, to symbolized the average values for the pressures of 10 bar and 30 bar, respectively. Finally the S_{10bar} and S_{30bar} means the experimental standard deviation extended to 95% of confidence. (All the pressures referred in this work are relative to the atmospheric pressure)

The Tab. 3.6, 3.8, 3.10 and 3.12 show the experimental values obtained for the *n'*(P) study, weather the Tab. 3.7, 3.9, 3.11 and 3.13, are used to summarize the most relevant values/information, and their values are plotted in graphic from 3.2 to 3.6.

- **Isooctane.**

Point	Relative Pressure (Bar)	Distance (mm)	Refrac. Index n'
0	0	0	1.387
1	5	2	1.386
2	10	5	1.385
3	30	15	1.381
4	10	6	1.384
5	30	16	1.380
6	10	8	1.384
7	30	18	1.380
8	10	7	1.384
9	30	17	1.380
10	10	8	1.384
11	30	18	1.380
12	10	9	1.383
13	30	19	1.379

Table3.6-Results of the n(P) study for Isooctane

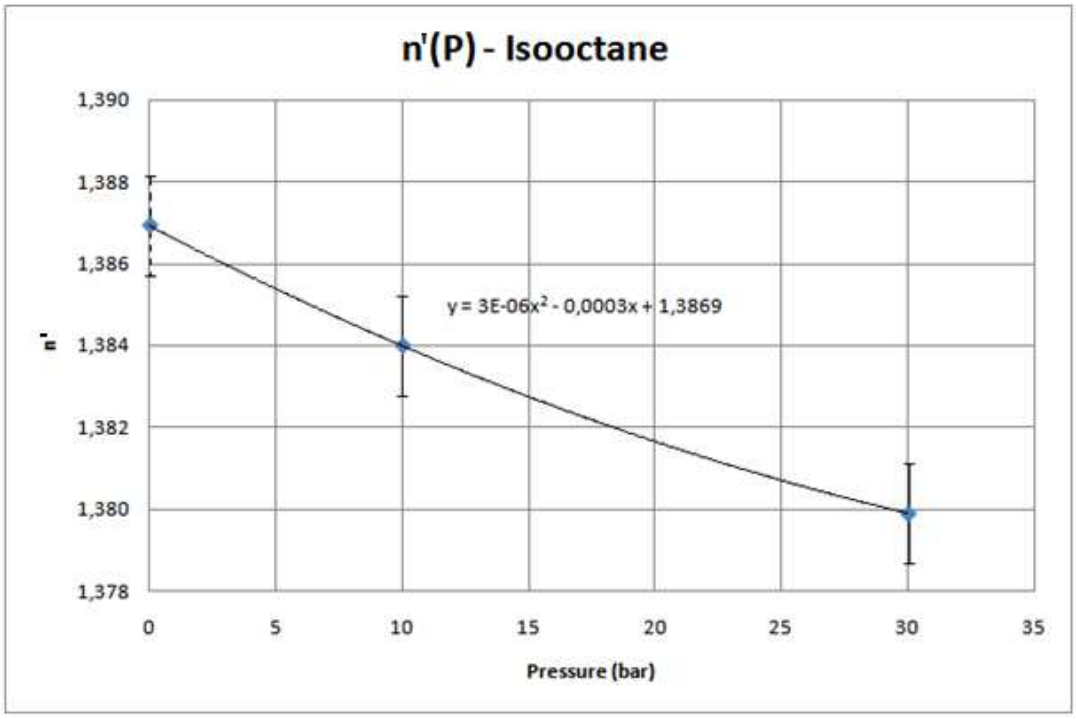

Graphyc3.2- Refractive index evolution of Isooctane with pressure

n'	n	$*n'_{10bar}$	s_{10bar}	$*n'_{30bar}$	s_{30bar}	$\Delta n/\Delta P$
1.387	1.369	1.3840	1,2E-03	1.3799	1.2E-03	-2.0E-04

Table 3.7-Resum results for Isooctane

From the values in tab.3.7 we verified that the refractive index decreases 0.0041 units when the pressure increases from 10 bar to 30 bar, which leads to a variation in the refractive index of approximately -0.0002 units per each bar.

As the extended standard deviation is 0.0012 bar^{-1} for both pressures, the range /interval of $\Delta n(P)$ could be extended to [-6.5E-3;-1.7E-3] leading to a slope ($\Delta n/\Delta P$) that can go from -0.0003 bar^{-1} to -0.00008 bar^{-1}.

The starting point (refer in graphic 3.2 as 0 bar) was not included in $\Delta n/\Delta P$ calculation manly because this measuring point was not repeated so its value is not so reliable as the other two, and this is also the reason why is represented in the graphics with interrupted dash.

- **E85**

Point	R. Pressure (Bar)	Distance (mm)	Refrac. Index n'
0	0	0	1.368
1	5	3	1.367
2	10	7	1.365
3	30	15	1.361
4	10	8	1.365
5	30	20	1.359
6	10	8	1.364
7	30	19	1.359
8	10	8	1.364
9	30	19	1.359
10	10	8	1.364
11	30	18	1.360

Table 3.8-Results of $n(P)$ for E85

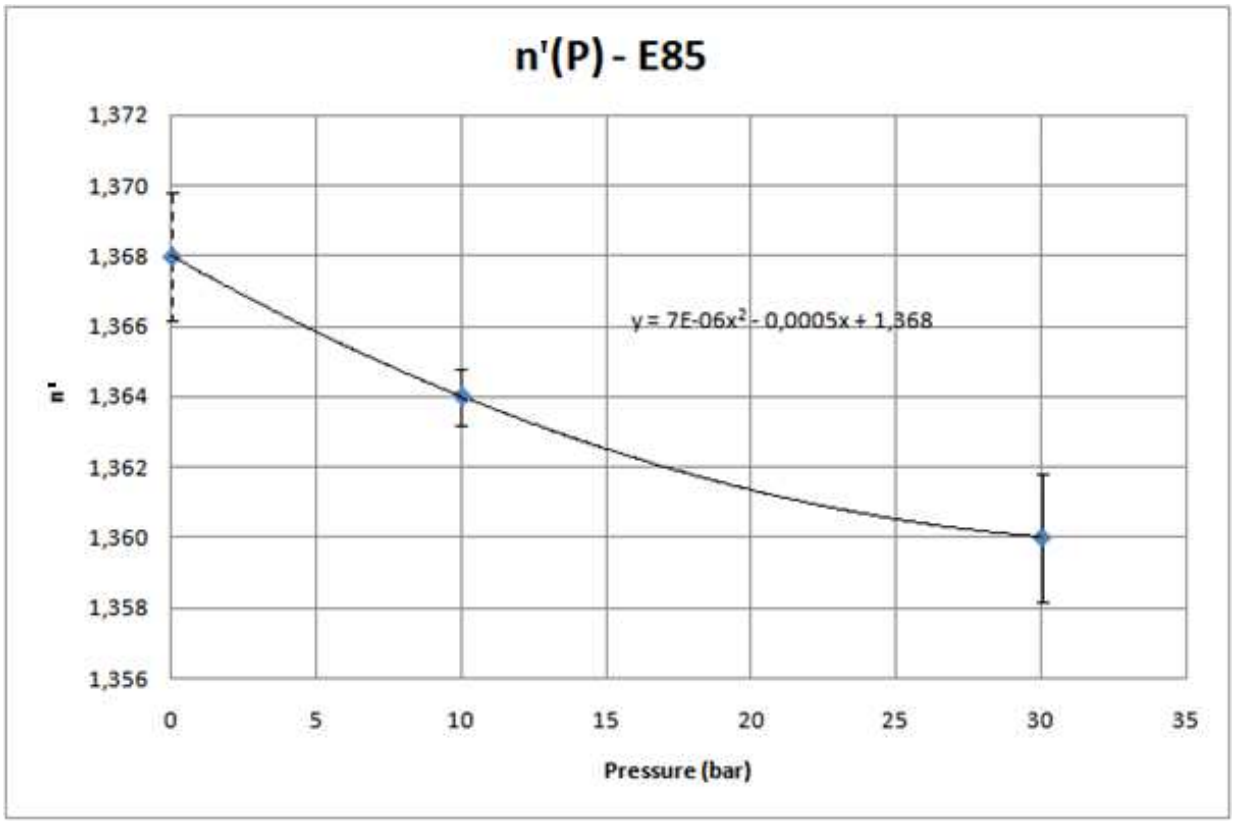

Graphic 3.3-Plot of the n(P) for E85

n'	n	$*n'_{10bar}$	s_{10bar}	$*n'_{30bar}$	s_{30bar}	$\Delta n/\Delta P$
1.368	1.366	1.3643	6.1E-04	1.3599	1.8E-03	-2.2E-04

Table 3.9-Resume of the values for E85

The variation of the refractive index from 10bar to 30bar is in the case of E85 of -0.004 units that gives a ratio of -0.00022 units per each bar if we approximate the two points for a straight line, which is a result slightly bigger than Isooctane (see tab.3.9).

The extended range for Δn in this case will be [6.41E-3; 1.59E-3] and so the slope can lea between -0.0003 bar^{-1} and -0.00008 bar^{-1}

- **E95**

Point	R. Pressure (Bar)	Distance (mm)	Refrac. Index n’
0	0	0	1.361
1	5	-	-
2	10	6	1.358
3	30	17	1.354
4	10	6	1.358
5	30	16	1.354
6	10	6	1.358
7	30	16	1.354
8	10	6	1.358
9	30	16	1.354
10	10	6	1.358
11	30	10	1.356

Table 3.10-Results of *n*(P) for E95

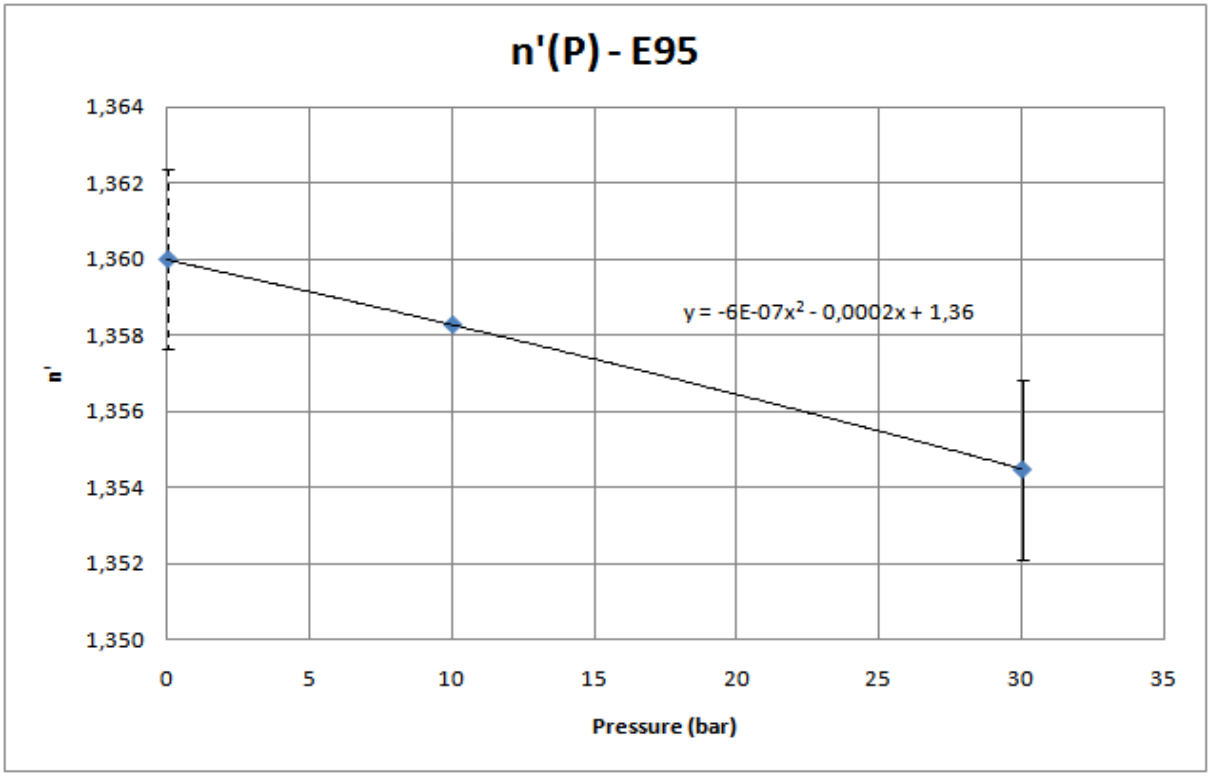

Graphic 3.5-Plot of *n*'(P) for E95

n'	n	$*n'_{10bar}$	s_{10bar}	$*n'_{30bar}$	s_{30bar}	$\Delta n/\Delta P$
1.361	1.360	1.3583	0.0E-4	1.3545	2.4E-04	-1.9E-04

Table3.11-Resum of the values for E95

The variation of the refractive index from 10bar to 30bar is in the case of E95 of -0.0038 units that give a ratio of -0.00019 units per each bar (see tab.3.11).

From tab.3.10 we can verify that curiously the refractive index for 10 bar is the same for all five measurements performed, given by that reason a null extended standard deviation. This result should be carefully analyze because is little probable that the measured value corresponds exactly to the real value (even with a null standard deviation).

The extended range for Δn in this case will be [4.04E-3; 3.56E-3] and so the slope can lea between -0.0002 bar^{-1} and -0.00018 bar^{-1}, (that corresponds to the smallest interval measured for the *n*(P) study).

- **Gasoline**

Point	R. Pressure (Bar)	Distance (mm)	Refrac. Index n'
0	0	0	1.428
1	5	2	1.427
2	10	4	1.426
3	30	16	1.422
4	10	8	1.425
5	30	18	1.421
6	10	6	1.425
7	30	17	1.421
8	10	6	1.425
9	30	16	1.421
10	10	1	1.426
11	30	15	1.422

Table 3.12-Results of the *n*(P) for Gasoline

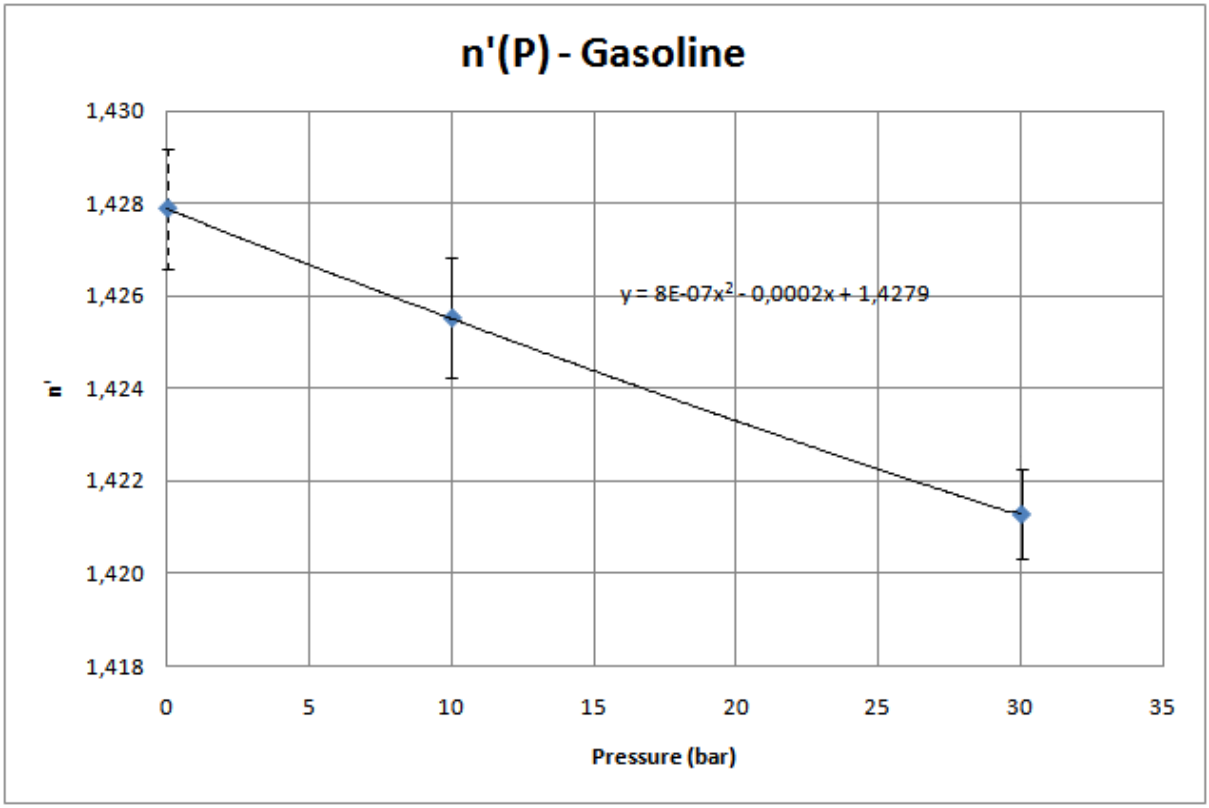

Graphic 3.6-Plot of the n(P) results for Gasoline

n'	*n*	$*n'_{10bar}$	s_{10bar}	$*n'_{30bar}$	s_{30bar}	$\Delta n/\Delta P$
1.428	1.429	1.4255	1.3E-03	1.4213	9.0E-04	-2.1E-04

Table 3.13 -Resume of the values for Gasoline

The variation of the refractive index from 10bar to 30bar is in the case of Gasoline of -0.0042 units that give a ratio of -0.00021 units per each bar (see tab.3.13).

The extended range for Δn in this case will be [6.4E-3; 2.0E-3] and so the slope can lea between -0.00032 bar^{-1} and -0.0001 bar^{-1}, (that corresponds to the smallest interval measured for the *n*(P) study).

3.2.6.2. Uncertainty Analyses

The usage of a pressure chamber was the cause of many others sources of errors. Not only the pressure fluctuations (and the difficulty to adjust it) was a source of errors, as also it caused another sources of errors, namely fluctuations in the refraction cell (once the metallic window is not completely attached to the chamber), and in the quartz windows.

The others sources of errors were: no direct measurement of the liquid temperature (and there is a noun uniform temperature on the refraction cell due to the air flow inside) and the composition changes due to the interaction between the liquid and the air, among others.

All these errors sources motivated a wick reproducibility of the measurements (at least if we compare to the *n*(T) measurements). The solution to outcome this problem was to repeat the measuring points (namely 10 and 30bar) several times and with this values calculate the average value of the refractive index (Eq.3.27) and the experimental standard deviation (Eq.3.28).

$$\bar{n}_P = \frac{\sum_{i=1}^{n} n_{Pi}}{N} \quad \text{(Eq.3.27)} \qquad S_{\bar{n}_P} = t \cdot \frac{1}{\mathrm{N}-1} \sqrt{\sum_{i=1}^{n} \left(n_{Pi} - \bar{n}_P \right)^2} \quad \text{(Eq.3.28)}$$

However not all the problems can be controlled, once there is no option to overcome the non direct liquid temperature measuring as also the pressure fluctuations inside the pressure chamber.

3.2.6.3. Conclusions

After analyzing the experimental results of *n*(P), the main conclusions we can extract are:

- From the observation of the Isooctane and E85 graphics we could be slightly tented to say that the *n*(P) evolution is quadratic, however we do not dispose of enough information to be shore of it, especially if we take into account the size of the extended standard deviation, and the small quadratic contribution. The quadratic contribution is 100 times smaller than the linear contribution and also 100 times smaller than standard deviation and this shows the lack information we have, to be able to conclude if there is any deviation from a linear behavior, so we can assume the *n*(P) as being a linear function.

- In opposition to what we expect the refractive index has decrease with the increasing in pressure. The only explanation to this fact is the higher sensitivity of air refractive index to pressure, i.e. the refractive index of air increases more than the refractive index of the fuel.

- The evolution of the *n* of air and fuel combined together, between the pressures of 10 and 30bar can be traduced by approximately -0.0002 bar^{-1} for all cases. As the effect is approximately the same for all fuels, and as we are measuring the combined effect of air and fuel, this could mean that the difference measured for the *n*(P) could be just motivated by the air refractive index change. If we think that the density might be the major effect on the *n*(P) we could easily accept that the change of the n(p) for liquids is neglected, since the increase in density with increasing pressure is much larger for air than for liquids. However to be able to draw further conclusions regarding the *n*(P) for the liquids we should separate the two effects.

We should remind, however that the results obtained for the combined effect might be more useful for PDA measurements, which is the main objective of this study, than the ones resulting from a isolated study effect of the *n*(P) on the fuel, once the refractive index used to measure the droplets size is the combined one.

3.2.6.4. Influence of the pressure on the refractive index of the fuel

To be able to know the impact of the *n*(P) on the liquid we should know how the refractive index of the air changes with pressure and how the physic phenomenon inside the chamber is unroll.

Air *n*(P)

In chapter 2.1 the Lorentz-Lorenz correlation for gases (Eq. 2.9) was presented. This equation together with Eq.1.10 can be used to easily calculate the *n*(P) for air if we assumed some simplifications. If we consider that Eq.2.9 can be approximated by Eq.3.29 (we can think on air as being a single component with R_{air} and ρ_{air} properties).

$$\frac{n^2-1}{n^2+2} \cong R_{air}.\rho_{air} \qquad \text{(Eq.3.29)}$$

If we despise the polarizability effect on the specific refraction R_i, it follows that this value will be a constant and the refractive index will be just dependent on the density effect. As the density can be easily correlated with pressure and temperature by the equation of perfect gases we will obtained in the end a direct correlation between Temperature and pressure. To calculate R_i we can use a known value for the refractive index of the air.

If we also Use the Edlén Equation, and for 25^{o}C, atmospheric pressure, air humidity of 50% and a wavelength of 514 nm the refractive index of the air according to [19] is 1.000268.

Then, using the referred values and assumptions it finally comes that the air refractive index for 10 bar is 1.002956 and 1.008329 for 30 bar (or 11 bar and 31 bar if we consider the absolute pressure, and considering also the atmospheric pressure as being equal to 1 bar). These are also the values that are obtained if we approximate *n*(P) for a straight line, passing by the zero pressure and one atmosphere.

Physic phenomenon inside the chamber

As the air has a double effect on changing the beam angle, i.e. the refractive index, first when is coming to the refraction cell and latter when it is coming out, and these two effects are influencing the *n* in opposite directions, we should verified the overall effect.

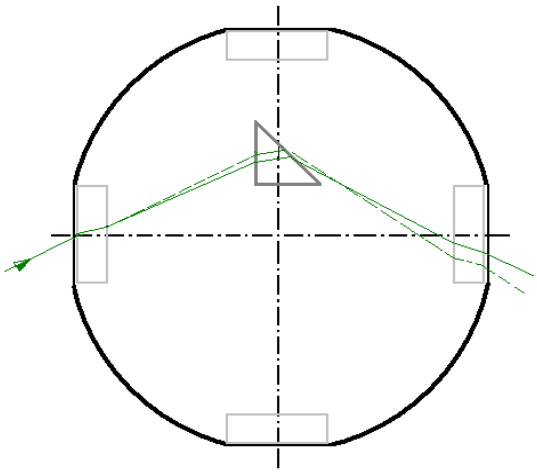

Figure 3.12- Physic phenomenon inside the chamber

In normal conditions of pressure the beam would be off-seated by the quartz glass and after being inside the chamber it would follow a parallel path to the original direction (i.e. before crossing the window) and the same will happen in its way out (see slashed dash in fig.3.12).

The described situation changes radically if we consider a gradient of pressures between the inside and the outside of the chamber. With the increase of pressure inside the camber the refractive index will increase and as the pressure outside still the same this will lead to a gradient in the refractive index.

For a higher pressure the incoming angle of a beam will be smaller and so the outgoing angle from the fuel will be slightly bigger. However this influence contra-balance the decrease of the outgoing angle (on the air), the influence of the increase of refractive index is much higher and so the outgoing beam will fallow in the left side of the original one, i.e. of the outgoing angle for no pressure. After crossing the quartz glass the outgoing angle will be slightly deflected to the right side (compare full and dashed lines in fig.3.12).

Results

Following the description of the physical phenomenon inside the chamber and using the same procedure presented 3.2.3.3 (scale approximation), we can estimate the *n*(P) effect in the measured liquids (tab.3.14).

Substance	T(°C)	P_0 (bar)	n	ΔP (bar)	$\Delta n_{combi.}$	$S_{\Delta n}$	$\Delta n_{separ.}$
Air[1]	25	1	1.000269	20	-	-	0.004
Isooctane[2]	25	1	1.387	20	0.0041	0.00E-4	≈0.001
E85[2]	25	1	1.366	20	0.0040	7.65E-4	≈0.001
E95[2]	25	1	1.360	20	0.0038	1.18E-3	≈0.001
Gasoline[2]	25	1	1.429	20	0.0042	3.24E-4	≈0.001

Table 3.14-Resume of the results from the separately study of *n*(P) for fuels and air.

[1]-The Δn_{sep} for air was obtained from subtraction of the presented values of the *n* for 11 and 31 bar,

[2] -The Δn_{sep} values for liquids were obtained by changing the refractive index of the fuel in the equation that describes the physical phenomenon inside the chamber until we match to the same values measured to the n(p) combined effect.

From the results the most critical values, in terms of its realability are for E95 because its extended deviation on Δp is of the same dimension of its Δn.

Conclusions

As referred previously the influence on the *n*(P) due to the liquid is much smaller than the influence due to the air, and approximately four times less .

The change of the refractive index for different liquids with pressure is approximately the same, and equal to 0.001±10E-3 per 20 bar (for the worst case), and it means that the composition does not have any influence on *n*(P).

3.2.5. Temperature Study

The ruler scale for temperature study used Methanol and Fluorobenzene as extreme reference values and Butanol as an intermediate reference, i.e. the scale was approximated by two straight lines.

3.2.5.1. Experimental Results

Isooctane

Point	Ref. Temp. (°C)	Rea. Temp. (°C)	Distance (mm)	Refrac. Index *n'*	Temperature (°C)	Refrac. Index *n*
0	25	25.0	0	1.390	30.9	1.390
1	40	38.9	16	1.383	40.2	1.386
2	60	56.3	36	1.374	59.2	1.376
3	80	74.4	56	1.365	78.1	1.367
4	100	92.4	77	1.356	-	-
5	40	38.9	16	1.383	-	-
6	25	25.0	0	1.390	-	-

Table 3.15-Results of the *n*(T) study for Isooctane

The values presented in tab.3.15 are referring to the results obtained in this experimental work (left side) and the results obtained in the first experimental work (right side). The match of the results is of the second decimal place, and if we consider a $\Delta n/\Delta T$ of 5.0E-4 $^{o}C^{-1}$ (the slope of the fitted curve in graphic 3.7) and convert *n* to the same temperature we obtained a maximum deviation between the values of *n* of 0.003.

According to the results obtained in this experimental work for an ΔT of 49.4°C the Δn is 0.025, for results from the experimental work 1 for a ΔT of 47.2oC the Δn is 0.023 and this gives approximately the same slope for the $\Delta n/\Delta T$.

T (°C)	*n'*	T (°C)	*n*
25.0	1.390	30.9	1.390

Table3.16-Comparison of the values for the *n* obtained in different Exp. work for Isooctane

Graphic 3.7-Plot of the *n'*(T) results for Isooctane

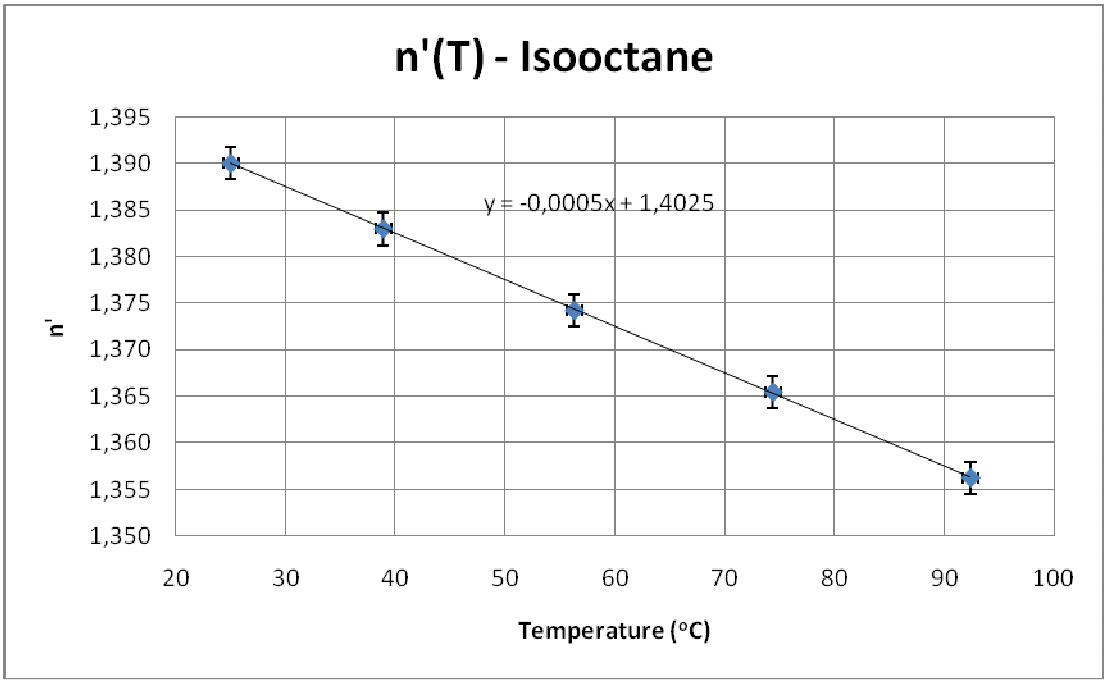

E85

Point	Ref. Temp. (°C)	Rea. Temp. (°C)	Distance (mm)	Refrac. Index n'
0	25	25.0	0	1.368
1	40	38,0	13	1.362
2	60	57.7	32	1.354
3	80	75.6	48	1.347
4	80	75.5	48	1.347
5	60	57.6	32	1.354
6	25	25.0	0	1.368

Table 3.17-Results of the *n'*(T) study for E85

The results of the *n*(T) evolution for E85 are presented in tab.3.17 and from them we can notice that for an ΔT of 50.6°C the Δn is 0.021, and as the starting and the end point are coincident the results are valid both for heating and cooling. The results of tab. 3.17 are presented in graphic 3.8

T (°C)	*n'*	T (°C)	*n*
25	1,368	26,3	1,366

Table 3.18- Comparison of the values for the *n* obtained in different Exp. work for E85

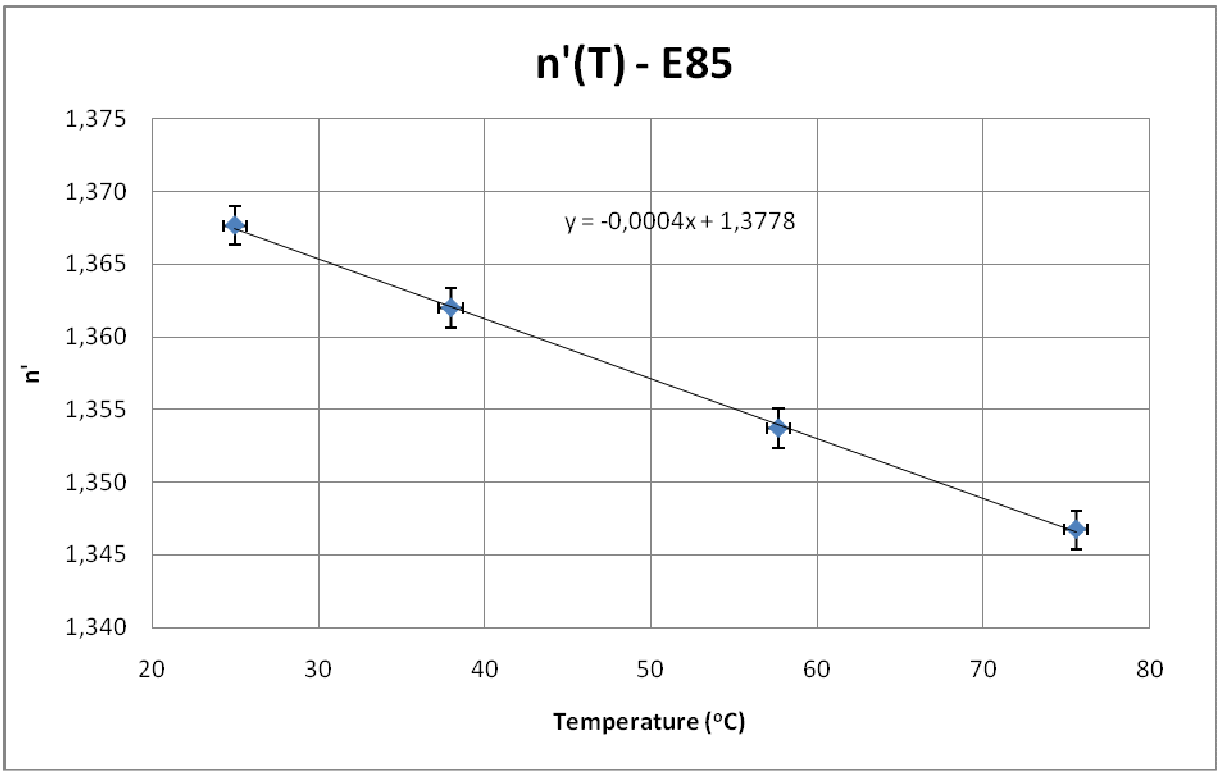

Graphic 3.8-Plot of the *n'*(T) results for E85

E95

Point	Ref. Temp. (°C)	Rea. Temp. (°C)	Distance (mm)	Refrac. Index *n'*
0	25	25.0	0	1.362
1	40	39.4	14	1.356
2	60	57.9	30	1.349
3	80	76.8	50	1.340
4	-	-	-	-
5	80	-	50	1.340
6	40	38.7	14	1.356
7	25	25.0	0	1.362

Table 3.19-Results from the n'(T) study for E95

For a *ΔT* of 51.8°C the *Δn* is 0.022, and this gives a slope for Δn / ΔT of 4.2E-4, which is very closed to the temperature derivative of the refractive index Δn / ΔT of the Methanol, which is 4.02 for a wavelength of 546.07 nm (see tab.3.19) and this confirm the results obtained. As the start and the ending point are the same there is no difference in *Δn/ Δn* between the heating and the cooling. In graphic 3.9 is presented the plot from the values of tab.3.19.

T (°C)	*n'*	T (°C)	*n*
25	1.362	26.2	1.360

Table 3.20- Comparison of the values for the n obtained in different Exp. work for E95

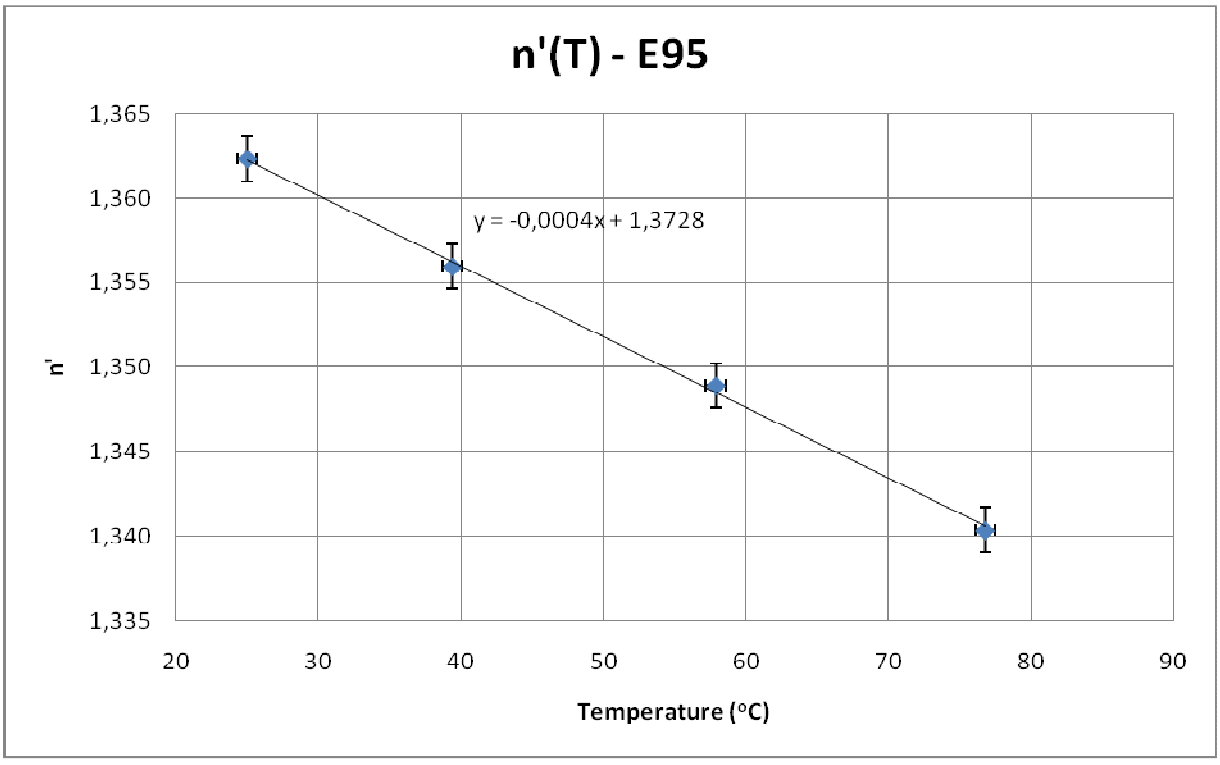

Graphic 3.9-Plot of the n'(T) results for E95

Gasoline

The values on tab. 3.21 establishe a comparasion between the resolts from the n(T) study for both Exp. Work 1 and 2.

Point	Ref. Temp. (°C)	Rea. Temp. (°C)	Distance (mm)	Refrac. Index n'	Temperature (°C)	Refrac. Index n
0	25	24.3	0	1.431	27.2	1.429
1	40	38.4	13	1.426	40.1	1.422
2	60	57.2	30	1.420	58.6	1.415
3	80	75.0	42	1.415	77.1	1.413
4	80	74.3	0	1.428	-	-
5	60	56.8	-24	1.437	-	-
6	40	38.1	-52	1.448	-	-
7	25	25.0	-72	1.456	33.9	1.438

Table 3.21-Results from the n'(T) study for Gasoline

For this case there is no complete match between the refractive index at 25°C "measured" and the resolting from the aproximation to the ruler scale. However the absolute values do not complitly match togheter the relative diference, i.e the total variation of the refractive index with temperature is the same and equal to 0.016. This observation is beased in the heating resolts, points from 0 to 3, and canot be compared to the colling curve. The results from the *n'*(T) are ploted in graphic 3.10.

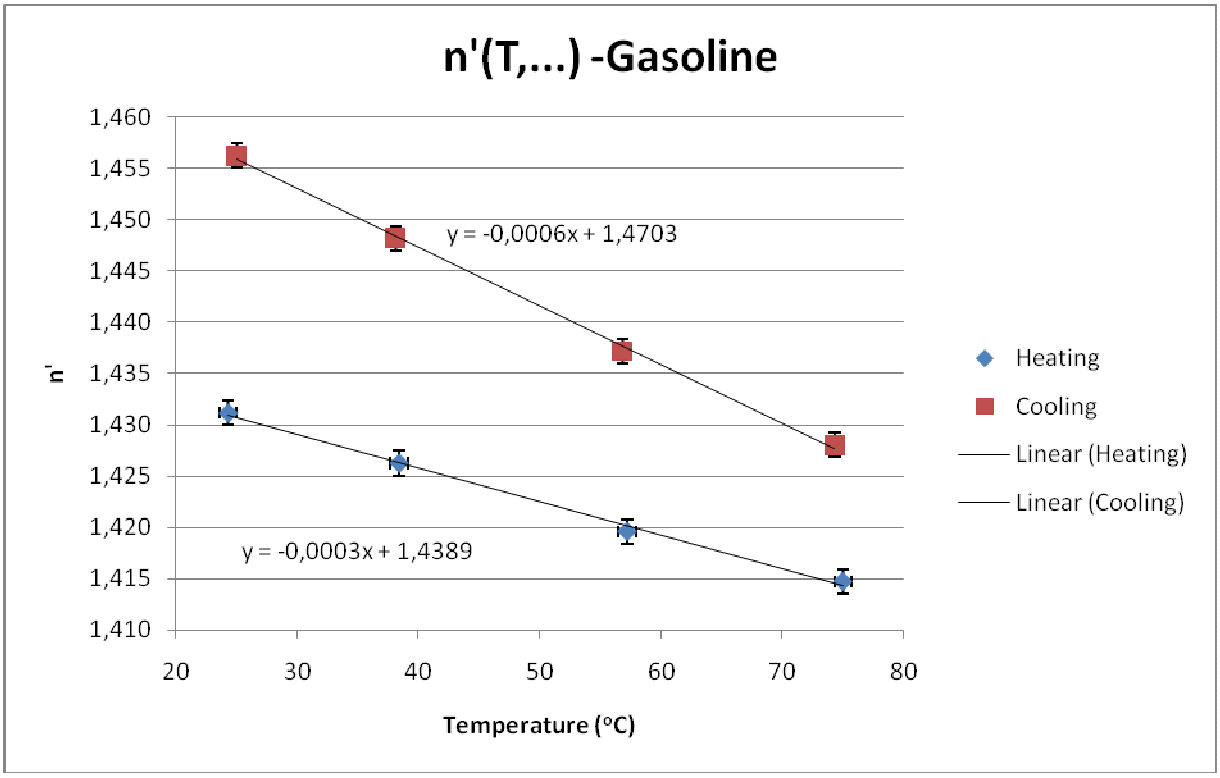

Graphic 3.10- Plot of the *n'*(T,...) results for Gasoline.

MCF1

Point	Ref. Temp. (°C)	Rea. Temp. (°C)	Distance (mm)	Refrac. Index n'
0	25	25.0	0	1.408
1	40	38.5	10	1.404
2	60	56.1	28	1.398
3	80	72.2	42	1.391
4	100	88.7	50	1.388
5	80	71.3	0	1.397
6	60	54.0	-22	1.406
7	40	37.4	-44	1.415
8	25	24.9	-63	1.422

Table 3.22-Results from the *n'*(T) study for Gasoline

The *Δn* for an *ΔT* of 63.7 °C is 0.017 for heating and 0.025 for cooling, and this shows that we have another case of composition change. The plot of the results from table 3.23 is presented in graphic 3.11.

T (°C)	n'	T (°C)	n
25	1,408	26,2	1,388

Table 3.23- Comparison of the values for the n obtained in different Exp. work for MCF1

Graphic 3.11- Plot of the *n'*(T,…) results for MCF1.

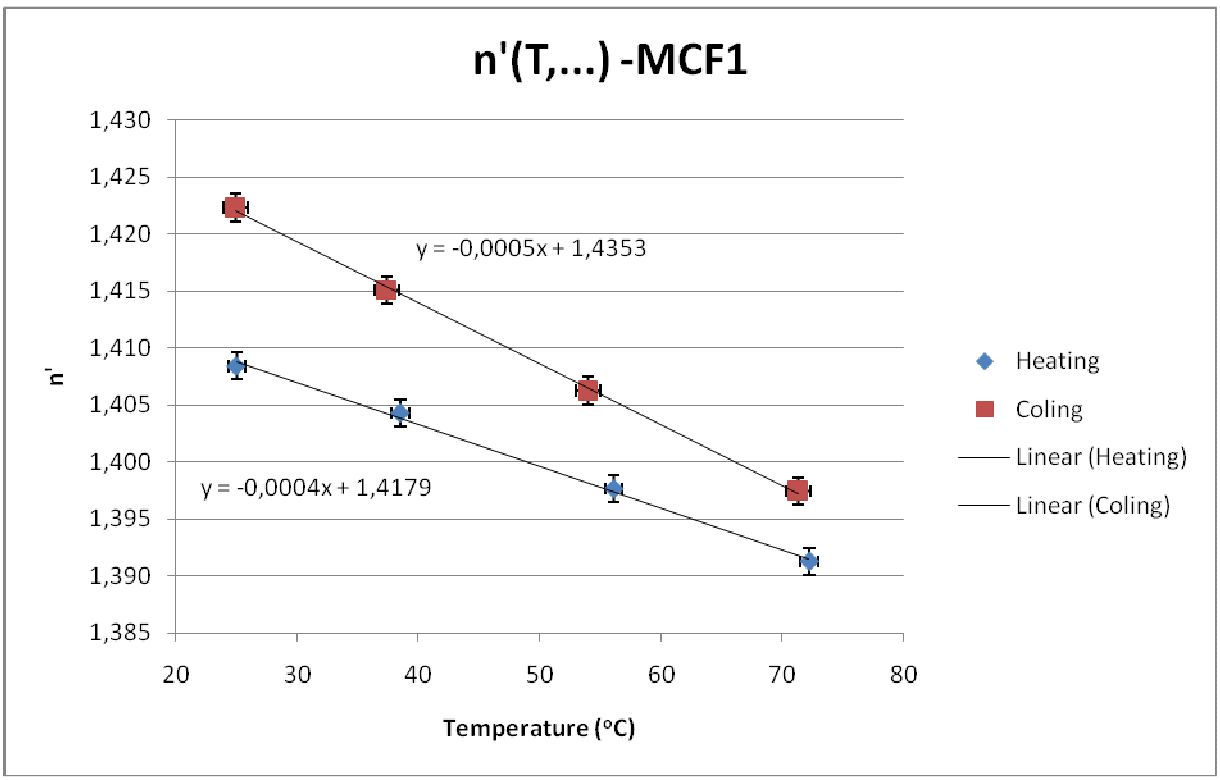

The representation of *n*(T) from Isooctane and MCF1, obtained in Exp. work 1 are now presented (graphic 3.12).

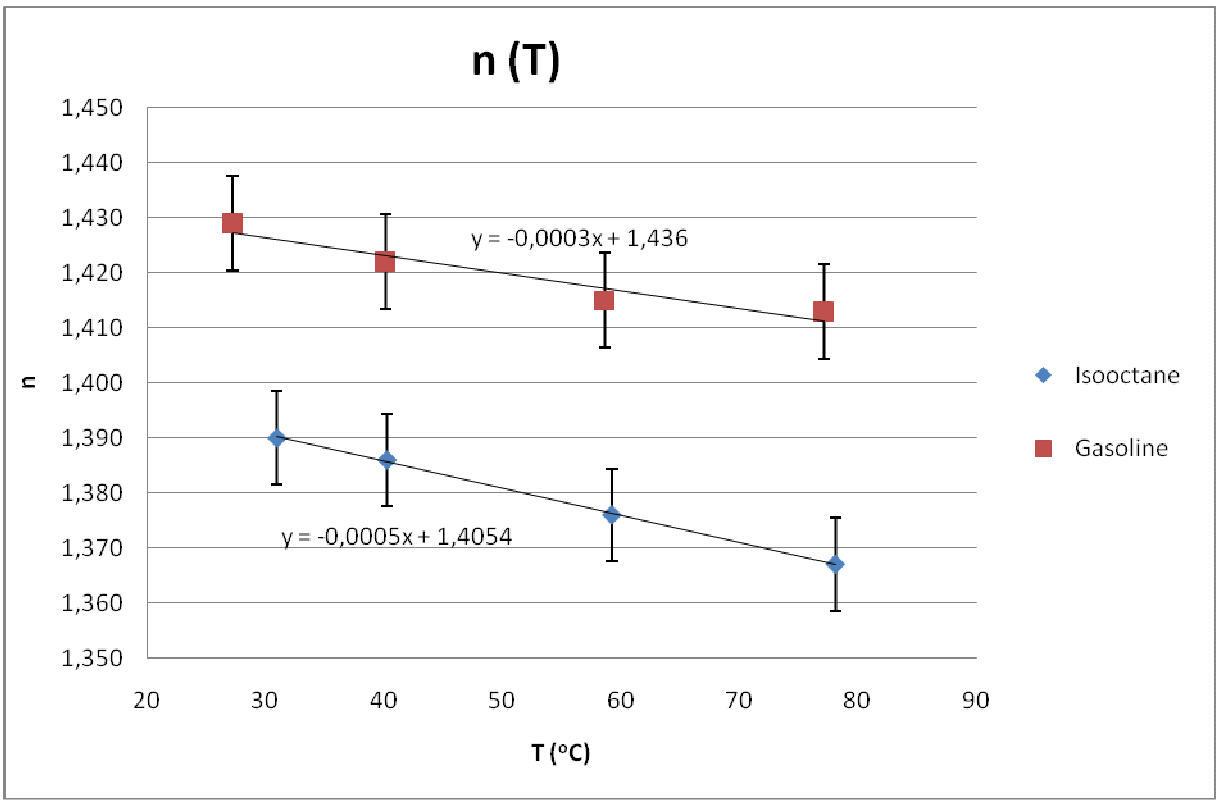

Graphic 3.12- Plot of the *n*(T) results for Gasoline and Isooctane from Exp. Work1.

3.2.5.2. Uncertainty analyses

The *n*(T) study in contrary of the *n*(P) study revealed a very reproducible experimental study, this means that there was no need to repeat several times the measuring points for a statistical analyzes. The main source of error for this experimental work is concerning the distance measuring of the points.

To estimated the uncertainty on *n*(T) determination we consider once again the ruler resolution *a*, and the point position $b_{posi.}$, to calculate the random error.

$$s = \frac{a}{\sqrt{3}} = 0.29\ \text{mm}$$

$$b_{resol._i} = s \cdot k = 0.29 \times 1.65 = 0.48\ mm$$

$$b_{posi.} = \pm 4\ \text{mm}$$

$$U_n = B_n = \sqrt{\sum_{i=1}^{n}\left(\frac{\partial n}{\partial x_i}\cdot b_{x_i}\right)^2} \qquad \text{(Eq.3.30)}$$

For the liquids falling on the Methanol-Butanol side, namely Isooctane, E85 and E95:

$$\frac{\partial n}{\partial x} = -4.39\times10^{-4}\ \text{mm}^{-1}$$

$$U_n = 1.77\times10^{-3}$$

For the liquids falling on the Butanol-Fluorobenzene side, namely Gasoline and MCF1:

$$\frac{\partial n}{\partial x} = -3.92\times10^{-3}\ \text{mm}^{-1}$$

$$U_n = 1.58\times10^{-3}$$

3.2.5.3. Conclusions

After analyzing the experimental results of *n*(T) the main conclusions we can extract are:

- In this study we can distinguish between three types of fuels according to their behavior,
  1. The single components as Isooctane that has a linear evolution of *n*(T) .
  2. The multi-components fuels that can be consider almost as a single fuel as E95 and E85 has an almost linear evolution.
  3. The multi-components like Gasoline and MCF1 that present a big difference between the heating and cooling curves and we cannot accurately estimate the *n*(T) evolution.
- Looking at the curves we can also see that the Isooctane ($\Delta n/\Delta T$=-5.0E-4) is more sensitive to the temperature variation than E85 and E95 (that present the same $\Delta n/\Delta T$ that is -3.0E-4).
- The last two points of the first conclusions are caused by the same effect, which is the composition change for multi-components fuels. In the 3rd point we mention that we could not estimate the *n*(T) effect and this is mainly because we are not just under the temperature influence but also under the composition change, this explains way we have one curve for heating and another for cooling leading to different refractive index. During the *n*(T) study the lighter components with low boiling points (starting at 25°C) start to evaporate and this increases the percentage

of the heavier components that, beside the higher boiling temperature, also present higher refractive index as is the case clear for the Aromatic Molecules in Gasoline (see graphic 2.1).

However for E85 and E95 the two curves were not noticed, but instead just a small deviation from the straight line approximation, and this is meanly because they composition are manly Ethanol, with 5% impurities for E95 and 15% of Gasoline for E85 (from which just a small part is lighter components) and so the composition just has a small effect.

3.3. Experimental work 3

3.3.1. Equipment

In this experimental work the equipment used were just a thermocouple calibrator, which was used as a heating device for liquids, and a thermocouple type K that was used to check the temperature of the liquid, all the rest of the experimental setup resumes to the usage of the same equipment and measurements procedure of the Exp. Work 1.

3.3.2. Description

The liquid was poured into a recipient and immersed into a water bath. Starting with room temperature we increased the water temperature until it reaches the temperatures of, 42^{o}C, 59^{o}C, 78^{o}C and finally 97^{o}C, after the temperature stabilized a sample from each temperature was taken and the time measured. This procedure was repeated for Gasoline and MCF1.

Later on and at room temperature (25^{o}C) the refractive index of each sample was measured, using the same setup as in Exp. Work 1.

3.3.3. Results

The results from the described measurements are presented in tab. 3.24, and with this experimental work we are trying to recreate the same composition change in the refractive index as the verified during the temperature study, and this is manly way we tried to heat up the liquids to the same temperatures studied previously; However as at the measuring time for each temperature the steady state for the liquid composition was not reached (fluid still evaporating) this same replication is something difficult to achieve once we have a variable affecting our measurements, that is the time and so we would

not have an exactly match between the composition evolution in Exp. work 2 and Exp. Work. 3.

Substance	Time (h:m:s)	Temperature (°C)	$\theta_{air\ out}$	U_θ	n	U_n
Gasoline	-	25	34.58	0,24	1.426	0.009
Gasoline	00:00:00	42	35.06	0,24	1.435	0.009
Gasoline	00:09:00	59	35.36	0,25	1.440	0.009
Gasoline	00:24:30	78	35.78	0.25	1.449	0.009
Gasoline	00:43:30	97	36.21	0.25	1.456	0.009
MCF1	00:00:00	25	33.64	0.24	1.408	0.009
MCF1	00:10:12	42	33.76	0.24	1.410	0.009
MCF1	00:34:04	59	33.92	0.24	1.413	0.009
MCF1	00:50:45	78	34.18	0.24	1.419	0.009
MCF1	01:10:00	97	34.47	0.24	1.424	0.009

Table 3.24-Results from the n(c) study

The total variation of the refractive index within the temperatures of 25°C up to 97°C is 0.03 for Gasoline and 0.016 for MCF1.

The time is definitely one important variable, but this study did not focus on having a precise study of the time influence but instead just used it as a reference.

Graphic 3.13-Plot of the results from n(C) study for Gasoline and MCF1

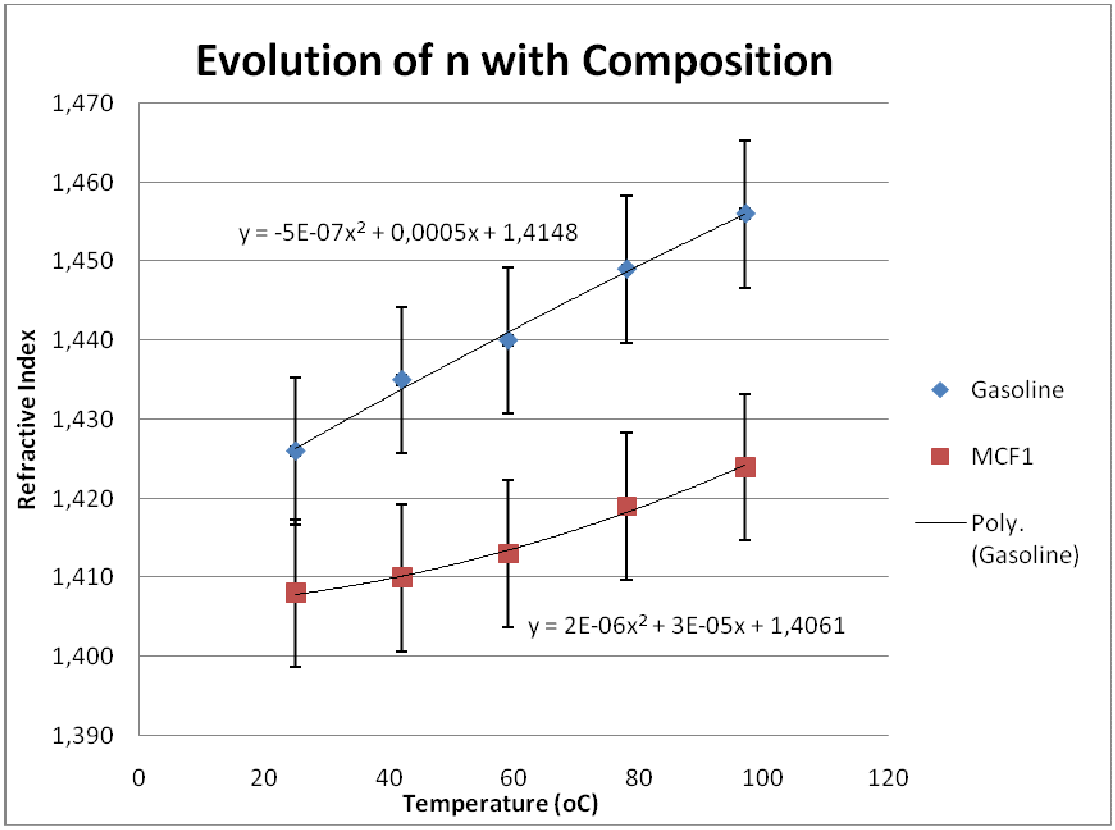

From graphic 3.13 we can see that the evolution of Gasoline is well fitted by a straight line (quadratic contribution approximately 100 times less than the linear factor) with a slope of 0.00003, we can also approximate the MCF1 curve by a straight line with a slope of 0.00005 but with a larger error (quadratic contribution approximately 100 times less than the linear).

3.3.4. Uncertainty analyses

The result of the uncertainty for this experimental work is presented in tab.3.24 and as we used the same procedure of Exp. Work 1 to measure the refractive index its calculation is exactly the same.

3.3.5. Conclusions

The first conclusion is the confirmation of something we expected, the refractive index of the liquid is increasing with the composition change.

The second and simple thing we find by viewing the results, which we also could predict before, is that the sensitivity of the refractive index to the composition change is bigger for Gasoline than for MCF1.

The gasoline is made majorly by Alkanes but also contain Aromatic Moleculs that have a bigger refractive index and a higher boiling point (see section 2.4), with evaporation the fraction of the Aromatic Moleculs increase leading to a bigger increase of *n* than the experienced by the MCF1 that is manly composed by Alkanes.

3.3.6. Comparison of Temperature and Composition effects

Gasoline

For the comparison of the results obtained for gasoline we used the results from Exp. work 1 (tab. 3.25).

Gasoline					
Heating		Cooling		Composition Only	
T (°C)	n	T (°C)	n	T (°C)	n
24.3	1.431	25.0	1.456	25	1.426
38.4	1.426	38.1	1.448	42	1.435
57.2	1.420	56.8	1.437	59	1.440
75.0	1.415	74.3	1.428	78	1.449

Table 3.25-Comparison of the results obtained for n(c) and n(T,..) for Gasoline

Although the starting points for the refractive index do not match perfectly, when compared to the same temperature range the composition effect on the refractive index Δn_{Toto} are approximately the same (0.023 for the n(T,…) study and 0.025 for the n(c)).

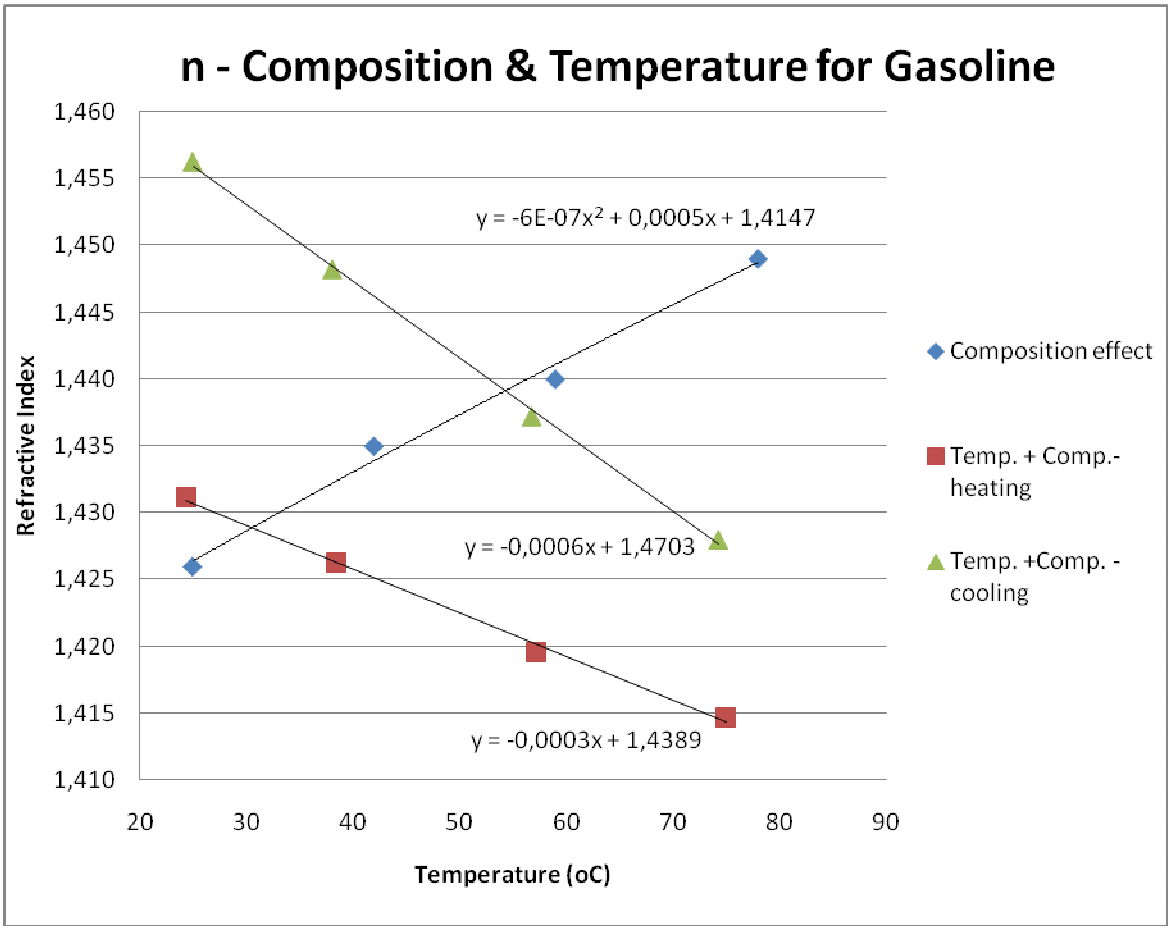

Graphic 3.14-Plot of the results from n(C) study and the n(T,…) for Gasoline.

Even knowing that the composition study does not represent the exact change verified during the *n*(T,..) study if we consider it sufficient to give an estimation of the isolated effect of the temperature on the refractive index for multi-components fuels , and also that the evolutions of *n*(T,..) heating can also be well represented by the approximated curves , we can use the equation from *n*(T,..) heating curve (Eq.3.31) to approximate the values of the refractive index obtained for both effects to the same temperature.

$$n = -3{,}0\times10^{-4}T + 1{,}4389 \qquad \text{(Eq.3.31)}$$

Unfortunately due to time and equipment limitations the study of composition could not be done for the same temperatures as in the *n*(T) study and this force us to assume this approximation to surpass this limitations.

Using the n(c) values and calculating the *n*(T) from the approximation equation for the same temperatures measured in n(c), we can calculate the total difference between n(T,..) and *n*(c) (tab.3.26), and assume this difference as being an estimation of the composition effect (due to the evaporation) on the evolution of *n*(T,..) for multi-components fuels (in this case Gasoline).

T (°C)	25	42	59	78	97
Δn	0.000	0.009	0.019	0.034	0.046

Table 3.26- Variation of n(T,..) due to the composition change for Gasoline

Finally as we have estimated the composition effect on *n*(T,..),we can used that values to plot the curve of the isolated effect of the temperature on the refractive index (graphic 3.15).

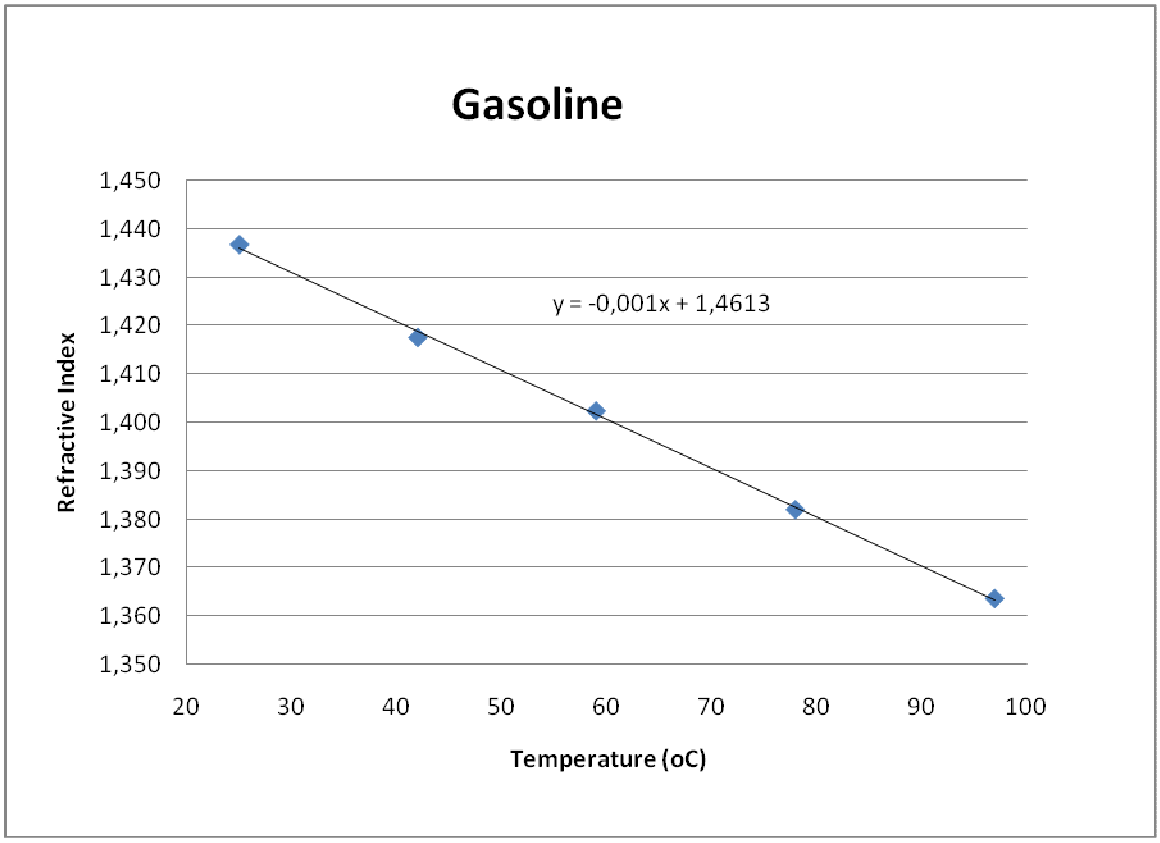

Graphic 3.15-Plot of the estimated curve of *n*(T) for Gasoline .

MCF1

The procedure used for MCF1 is the same presented for Gasoline, and the comparison of the values as also their plot are presented in tab. 3.27 and Graphic 3.16.

MCF1					
Heating		Cooling		Composition Only	
T (^{o}C)	*n*	T (^{o}C)	*n*	T (^{o}C)	*n*
25.0	1.408	24.9	1.422	25	1.408
38.5	1.404	37.4	1.415	42	1.410
56.1	1.398	54.0	1.406	59	1.413
72.2	1.391	71.3	1.397	78	1.419

Table 3.27-Comparison of the results obtained for n(c) and *n*(T,..) for MCF1

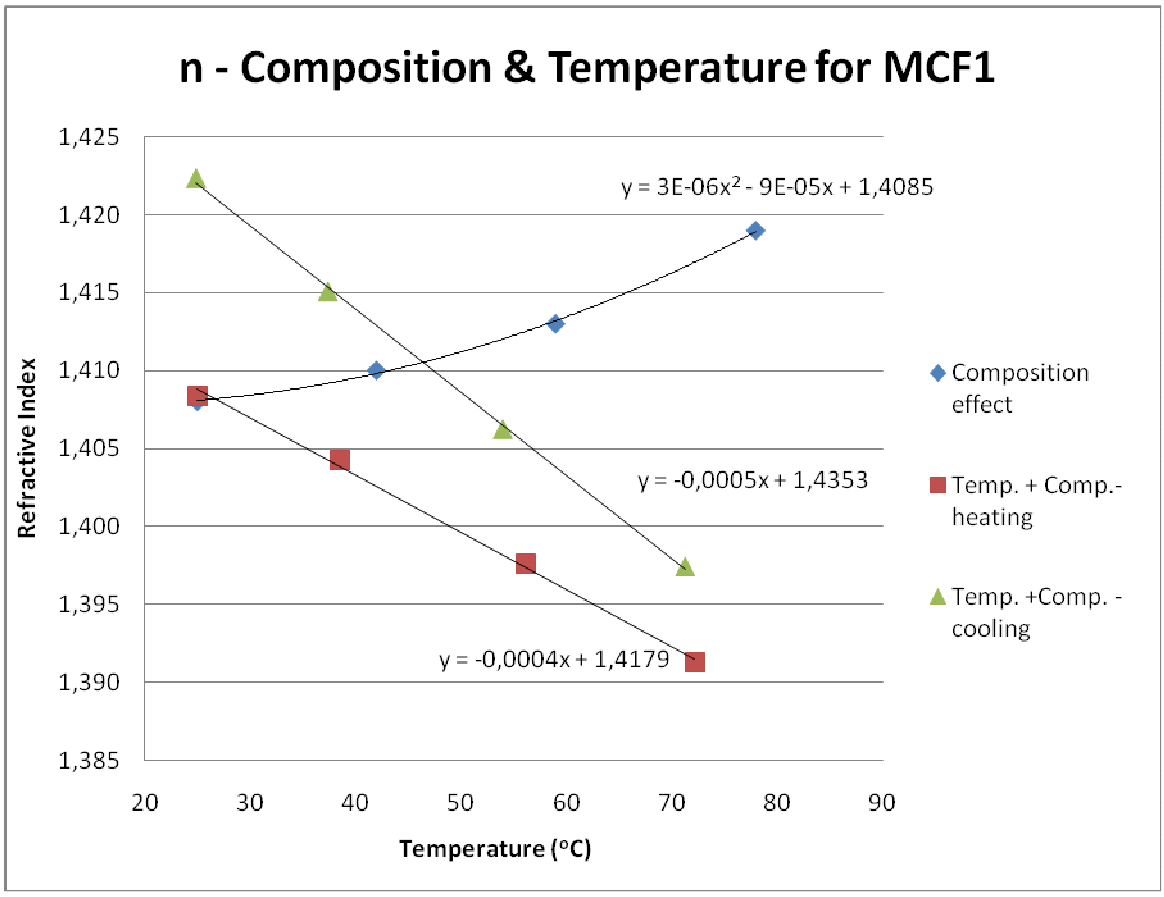

Graphic 3.16-Plot of the results from n(C) study and the *n*(T,...) for Gasoline.

From the comparison of the Graphic 3.14 with Graphic 3.16 we notice that the $\Delta n/\Delta T$ during the heating is lower for gasoline than for MCF1.

T (°C)	25	42	59	78	97
Δn	0,000	0,009	0,019	0,032	0,045

Table 3.28- Variation of n(T,..) due to the composition change for MCF1

The variation due to the composition is bigger for Gasoline (tab.3.28) than for MCF1 (tab. 3.26), and this is something that we should expect as MCF1 is only made by Alkanes and the Gasoline is majorly made by Alkanes but also have Aromatic Molecules with higher refractive index, as it was also said before.

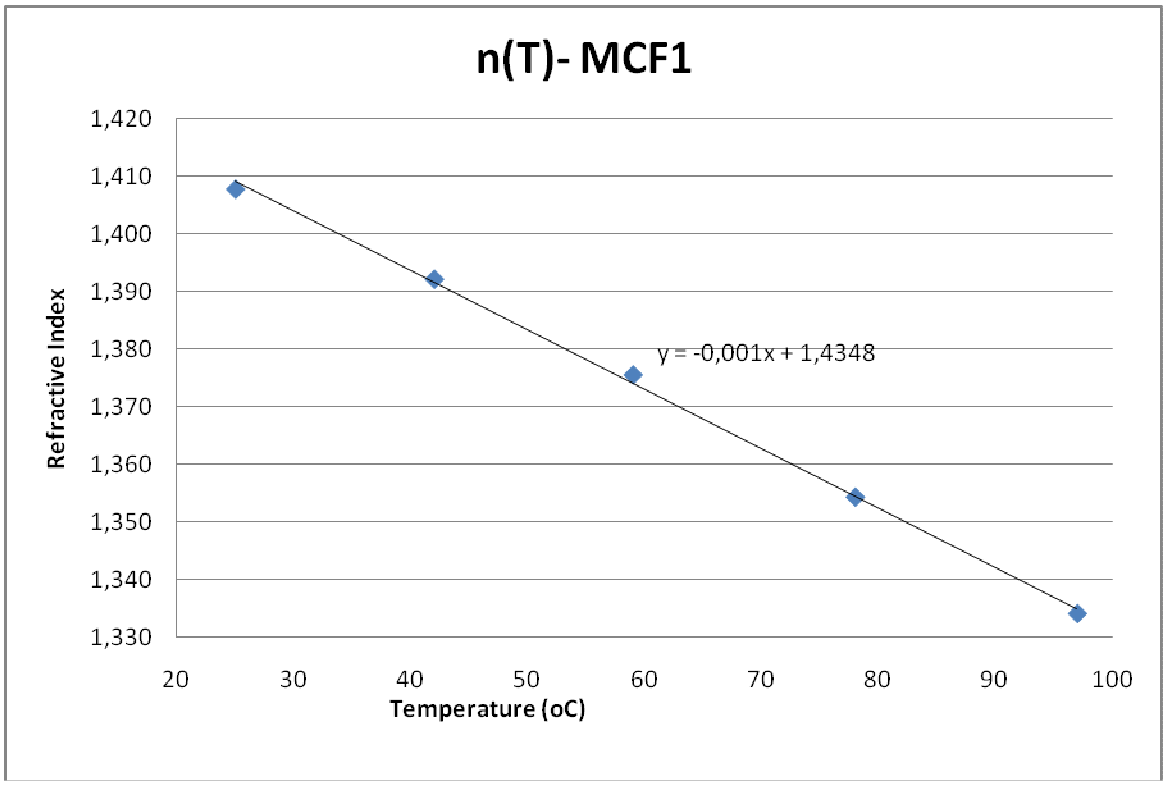

Graphic 3.17-Plot of the estimated curve of *n*(T) for MCF1 .

The last two points contra-balance each other leading to a final dependence of the refractive index from the temperature equal for both cases (see slope of graphic 3.16 and graphic 3.17). Which is something that we can easily accept as the major composition of both fuels is based in Alkanes.

4. Case Study PDA study

The second main objective of this Thesis was to understand the importance/influence of the refractive index precision on the particle size measuring, according to the results obtained in the first part of the work.

With that purpose some measurements with PDA using different precisions for the *n* were planed. Unfortunately due to the unavailability of the equipment it was impossible. To outpace this obstacle a correlation of the particle size and the refractive index *n* presented by Eq.2.13 was used (to be more easy to the reader the equation is again showed).

$$\Phi_{refraction} = \frac{2\pi d_p}{\lambda} \frac{n_{rel}\sin\theta\sin\psi}{\sqrt{2(1-\cos\theta\cos\psi\cos\varphi)(1+n_{rel}^2-n_{rel}\sqrt{2(1+\cos\theta\cos\psi\cos\varphi)})}}$$

However this correlation is in the bases of the algorithm used by the PDA equipment to measure the particle size, we should be aware of the differences, and this means that the values obtained using the presented equation should be seen just as reference, which should be confirmed later with the PDA measurements.

The values used for the equation parameters are near to the typical values used and are presented in Tab.4.1. The obtained results are presented in Tab.4.2.

λ	θ	ψ	φ	Φ	n_{air}
514 nm	6.9 °	9.74 °	68.8 °	-9.85°	1.000

Table 4.1-Values o the PDA parameters used to calculate the droplet size

n	1.3	1.36	1.37	1.374	1.375
d (µm)	20.000	20.151	20.182	20.194	20.197

Table 4.2 Values from the *D*(n) for PDA

For the values presented it seems that the refractive index accuracy does not change the determined particle diameter much, which is an unexpected conclusion. It have been reviewed at [9] the importance of the refractive index for accurate measurements and even the angles that should be used to reduce that effect, but unfortunately without presenting values.

To confirm the previous values other equation (eq.3.1) found in the literature [19] was used but once again the same values were obtained.

$$\Phi_{refraction} = \frac{4\pi\, d\, n_{air}}{\lambda}\left\{\sqrt{1+n_{fuel}^2-\sqrt{2}\, n_{fuel}\sqrt{1+\sin\theta\sin\varphi\sin\Psi+\cos\theta\cos\varphi}}-\right. \quad \text{(Eq.3.1)}$$
$$\left.\sqrt{1+n_{fuel}^2-\sqrt{2}\, \mathrm{n}_{\mathrm{fuel}}\sqrt{1-\sin\theta\sin\varphi\sin\varphi\sin\psi+\cos\theta\cos\varphi}}\right\}$$

5. Final Conclusions

We have designed equipment to measure the refractive index of fuels at temperatures and pressures corresponding to the conditions in a Combustion Engine, and the values obtained have enough accuracy to be used as an input parameter for Future Drops Size measurements in fuel sprays with PDA.

The refractive Index of fuels were studied as a function of Pressure Temperature and Composition, the parameters having the strongest influence on the refractive index and thereby on the droplets size measurement in fuel sprays.

For the pressure study we conclude that for both air and liquid the refractive index is increasing with pressure, however as the increasing refractive index of air is lager the combined effect lead to an apparent linear decrease of the refractive index of the fuel.

For the temperature study we conclude that the refractive index is decreasing with the increasing temperature. For single components and fuels dominated by one compound, e.g. E85, the *n*(T) is a linear function. For multi-components the evolution of *n*(T) have reveal not reversible, i.e. different values were obtained during heating and cooling.

The non reversible values obtained for the multi-components fuels were suspected to be caused by a change in composition, due to the evaporation of the lighter components. This assumption was confirmed by measuring the influence on the *n* by the composition change caused by heating. The composition change due to the evaporation causes an increase of the refractive index which counteracts the effect of the temperature.

6. Future Work

Depending on how deep are our interests on this subject are we can establish different objectives for a Future work, but depending on the priority they should focus on confirmation of some results, namely:

- To confirm the importance of the refractive index for PDA measurements using the PDA system. For example, measurements can be carried out at identical spray

conditions, varying the n given as input for the drop size calculation and register the difference in particle diameters obtained for various *n*;

- To confirm the values obtained for the refractive index, at room temperature and atmospheric pressure, using for example an Abbé refractometer;
- Repeat the refractive index study for the combined effect of temperature and pressure, verify the total influence in it and finally compare to the conclusions that were taken from this work.
- Once the temperature of a droplet during the injection is difficult to predict we should try to recreate the same conditions by changing the inlet temperature of the air that comes into the chamber and with this conditions repeat the *n*(T) measurements and this time we can also combine with the pressure effect.
- To make the study more reliable a detail study of the composition affect on the refractive index, and this implies a composition analyses of the sample for different temperatures and also taking into account the time factor, should be held.

Obviously the last tree objectives only are worthwhile, at least in what concerns the PDA system, if the refractive index reveals as an important parameter that could affect the particle measuring.

If a more deep study is desired we can continue to the molecular scale and study the molecular structures and interactions and correlate their proprieties with the refractive index. This study could start by analyzing the Lorentz-Lorenz correlation and the electronic polarizability of the molecules, which were presented in this Thesis.

We should also refer that this study can also be important for other techniques that are dependent on using the refractive index.

7. References

[1]-G.H. Meeteen – Schlumberger Cambridge Research.

[2]-Hecht and A. Zajac - Optics, Addison –Wesley, Reading.MA. 1974.

[3]-Emil Reisler, Henryk Eisenberg and Allen P.Minton.Temperature and Density Dependence of the Refractive Index of Pure Liquids. Polymer Dept. , The Weizmann Institute of Science, Rehovot, Israel and National Institute of Artrities and Metabolic Diseases, Bethesda, Maryland. Journal of the Chemical Society-Faraday Transactions II, January 1972.

[4]-en.wikipedia.org/wiki/Polarizability-12/05/07

[5]-James C. Ownes. Optical Refractive Index of Air: Dependence on Pressure, Temperature and Composition. January 1967/Vol.6, No.1/Applied Optics.

[7]-Albercht, H.-E., M. Borys, N.Damaschke, and and C. Tropea, Laser Doppler and Phase Doppler Measurement Techniques: Springer-Verlag. 2003.

[6]- Katharine Kohse-Hönghaus and Jay B. Jeffries, Applied Combustion Diagnostics

[8]-www.dantecdynamics.com/Defaut.aspx?ID=1058-05/07/20

[9]- Doctorial Thesis: Ronny Lindgren, Characterization of Gasoline of Gasoline Spray-Wall Interactions, Division of Thermo and Fluid Dynamics of Technology, Chalmers University of Technology, 2004.

[10]- Heywood, John B., Internal combustion engine fundamentals.

[11]-Doctorial Thesis: Mikael Skogsberg- “A Study on Spray-Guided Stratified Charge Systems for Gasoline DI Engine” – Department of Applied Mechanics, Chalmers University of Technology, 2007.

[12]-www.spi.se/produkter.asp?art=47-10/07/08

[13]-www.spi.se/produkter.asp?art=48-10/07/08

[14]- OKQ8 Ethanol E85- Säkerhetsdatablad-2005-12-02.

[15]-www.hbcpnetbase.com - ”Handbook of Chemistry and Physics”-88th Edition 2007-2008.

[16]- Hauf, W. and Grigull, U., Optical Methods in Heat Transfer (Academic Press, New York, 1950)

[17]-Hugh W. Coleman and W. Glenn Steele, Jr – Experimentation and Uncertainty Analysis for Engineers.

[18]- http://emtoolbox.nist.gov/Wavelenght/Abstract.asp.-10/06/08

[19]-Lusty, M.E. and Dunn, M.H., Appl. Phys. B 44, 193 (1987).

Acknowledgments

First of all I should confessed that in the end, to work in this project research at Chalmers have raveled an wonderful experience, and manly because of the contribution of everyone around, even the ones not directly involved in the project, as Alf Hugo, Savo, Rolf, etc. and I take this chance to show by now my great gratitude to them.
I also would like to present some particular acknowledgments to,
Professor Ingemar Denbratt for well receiving me at Chalmers Combustion division, allowing me to make this research work, showing interest in our work and being very comprehensive every time a new problem shows up.
Professor Mats Anderson that have been one of the biggest mentors of this project and that had follow my work since the beginning until the end, abdicating of some hours with his family to help me, reviling not just a supervisor but also a friend and for what I am really grateful.
PHD Student Stina Hemdal for spending many hours with me in the Lab and for following me in this work and giving me support in everything she could.
Research Engineer Torbjörn Cima for all his technical support and extra time spent in this work, also reveling very important for my social integration. I am grateful for his truly friendship.
Technical staff from the Work shop (Ingemar Johansson and Morgan Svensson) and also Bo Peterson and Lars Jernqvist for their technical support and by their generosity and kindness.
Finally I would like to thank PhD Student Raúl Ochoterena for his critical friendship that has helped me growing in many aspects.

All these people will make my departure from Sweden harder!

Appendix 1

Pt_{100}		Type K			
R (mΩ)	T (°C)	T (°C)	U_{Pt100}	ΔT	U_{Total}
109,48	24,3	23,6	0,1	0,7	0,7
114,88	38,3	39,0	0,1	-0,7	0,7
122,23	57,4	57,7	0,1	-0,3	0,3
129,07	75,2	75,6	0,1	-0,4	0,4

Table 1.a-Values from the calibration of the thermocouple K against a Pt100

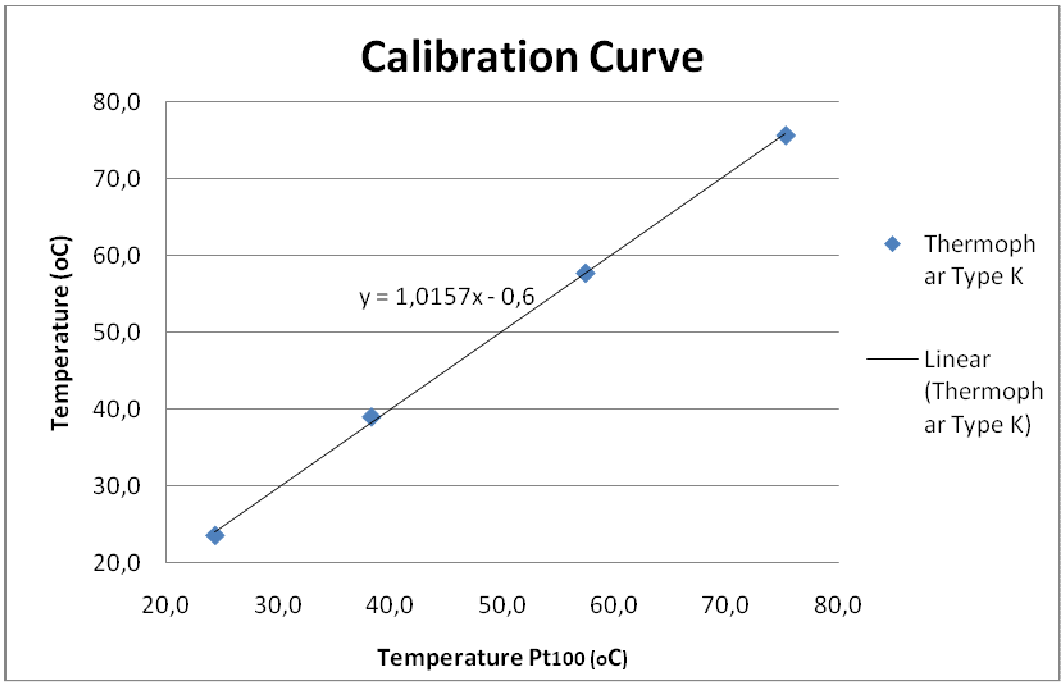

Graphic.1.a- Thermophar Calibration Curve

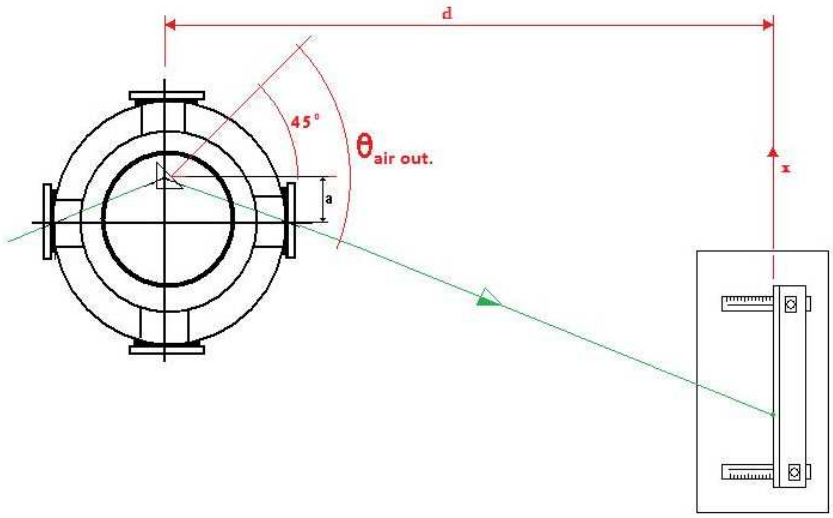

Fig.1.a -Schematic representation of the measuring method